Jan Staněk

K Laterálním Interakcím v Samoorganizovaných Monomolekulárních Vrstvách

TOWARDS LATERAL INTERACTIONS WITHIN SELF-ORGANIZED MONOMOLECULAR LAYERS

Diplomová práce

Vedoucí diplomové práce: Tomáš Baše, Ph.D.

Praha 2018

Prohlášení

Prohlašuji, že jsem tuto závěrečnou práci zpracoval samostatně a že jsem uvedl všechny použité informační zdroje a literaturu. Tato práce ani její podstatná část nebyla předložena k získání jiného nebo stejného akademického titulu.

Jsem si vědom toho, že případné využití výsledků, získaných v této práci, mimo Univerzitu Karlovu a Ústav anorganické chemie Akademie věd České republiky je možné pouze po písemném souhlasu těchto institucí.

V Praze dne 14. srpna 2018.

Poděkování

Obsah/Summary

Abbreviations and Constants

AO - Atomic Orbital
AT - Alkanethiol
BE -Binding Energy
CPS - Counts Per Second
EAL – Effective Attenuated Length
EM - Electromagnetic
FTIR - Fourier Transformation Infrared Spectroscopy
KE -Kinetic Energy
IMFP -Inelastic Mean Free Path
M1 - 1-SH-*meta*-carborane
M9 - 9-SH-*meta*-carborane
M1-COOH - 1-COOH-7-SH-*meta*-carborane
M9-COOH - 1-COOH-9-SH-*meta*-carborane
MO - Molecular Orbital
n.n.d. - nearest neighbor distance
O1,2 - 1,2-$(SH)_2$-*ortho*-carborane
O9,12 - 9,12-$(SH)_2$-*ortho*-carborane
P1-COOH -
PE - Photoelectron
RSF - Relative Sensitivity Factor
SAM - Self Assembled Monolayers
STM - Scanning Tunneling Microscopy
TF - Transmission Function
UHV - Ultra High Vacuum
VdW - Van der Waals
XPS - X-ray Photoelectron Spectroscopy

$N_A = 6.022140857 \cdot 10^{23}$ [mol^{-1}]
$\varepsilon_0 = 8.854187817 \cdot 10^{-12}$ [$F \cdot m^{-1}$]
$h = 6.626070040 \cdot 10^{-34}$ [$J \cdot s$]

Van der Waals atomic radii:
r(hydrogen) = 1.20 Å
r(carbon) = 1.70 Å
r(oxygen) = 1.52 Å
r(sulfur) = 1.80 Å

Abstract

This work aimed at the utilization of chemical principles for stabilization of self-assembled monolayers (SAMs) of carboranethiol derivatives on a flat gold surface. Ideas employing surface confined coordination complex formation and dipole-dipole intermolecular interactions were outlined and the respective literature survey was compiled. Preliminary experiments were carried out to test for their feasibility and surfaces modified with self assembled monolayers proved very sensitive to reaction conditions ordinarily used for bulk synthesis. The chemical sensitivity of the studied surfaces, the necessity of using appropriate surface-sensitive analytical techniques and the depth of the problem initially defined made this task both advanced and challenging. The formation of intermolecular coordination complexes with ω-carboxylated SAMs of *meta*-carborane-9-thiol was chosen to answer those issues, extending the previous work of the author on carboxylated carboranethiol isomers presented in his bachelor thesis. Concepts different of those based on coordination chemistry are briefly discussed as well, but more as prospects for future work and to present this work in a broader context to which it belongs.

Characterization of molecules assembled on a surface in a single layer requires surface sensitive techniques, for the number of molecules per surface area is relatively small. For example a SAM of 1-carboxy-*meta*-carborane-9-thiol on gold flat surface contains less than a nanomole per cm^2. X-ray photoelectron spectroscopy (XPS) was used as a convenient method for this study, not only as a tool for qualitative analysis as is common in the literature on SAMs, but also to asses some quantitative information on the formation of surface confined metal complexes. Discussion on some specific difficulties stemming from quantitative XPS analysis of SAMs is provided in this thesis. Dynamic contact angle measurements were used as means of probing the qualitative changes in the preliminary experiments.

Introduction

Self assembled monolayers

First report of a SAM on a solid surface was published by Zisman *et al.* in 1946, who observed reversible adsorption of polar amphiphilic compounds on metal and glass surfaces and investigated the monolayer formation by contact angle measurements. The phenomenon was examined for molecules containing either −OH, −NH$_2$ or −COOH anchoring groups and an aliphatic tail, the anchor interacting with the bare surface and the tail pointing away from the substrate, determining its wetting properties.[1]

SAM is a spontaneously formed, structurally ordered molecular assembly of a surfactant adsorbed on a surface. The adsorption is primarily driven by the affinity of an anchoring group to a substrate surface and additionally by lateral intermolecular interactions between the SAM constituents, together governing the density of molecules on the surface and the structure of the adsorbed monolayer.

Depending on the nature of the anchor-substrate interaction, molecules may be classified either as chemisorbed, when covalently bonded to the substrate, or physisorbed, when bound to the surface only through weak electrostatic forces, Van der Walls intermolecular forces or hydrogen bonding. The difference between chemisorbed and physisorbed molecules may also be roughly expressed by interaction enthalpy, as $\Delta H < 42$ kJ/mol for physisorbed molecules and $\Delta H > 42$ kJ/mol for chemisorbed molecules.

The range of applicable anchoring groups and complementary surfaces has been extended since the opening studies, some of the known systems available for chemisorption of SAMs are listed in **Table 1**. The list presents selected examples to demonstrate the possibilities for surface binding of molecules into structures with a certain degree of order midst the adsorbed molecules.

Almost any molecule may bear an appropriate anchor and be used as a SAM constituent. The range of applicable molecules thus spans over aliphatic as well as aromatic molecules containing cycles, heteroatoms and additional functional groups. The surface structure of a monolayer is driven by both the density of substrate binding sites suitable for substrate-anchor interaction and the lateral intermolecular interactions between the SAM constituents, making the surface structure dependent on the nature of the molecular backbone.

Substrate	Anchoring group	Anchor bonding	Notes
Au[1,2]	thiol, disulfide (analogously selenols)	−S−Mt− (−Se−Mt−)	thiolates on Au are usually stable, well defined, densely packed SAMs; physisorbed species my coexist alongside chemisorbed
other substrates (transition metals[1], GaAs[1,2], InP[1,2], CdSe[2], ZnSe[2], ITO[2]...)	thiol, disulfide	−S−Mt−	−
usually Au and other coinage metals[1]	other sulfur containing species (dialkylsulfide, xanthate, thiocarbamate...)	−	−
Ag[1,2], AgO[1], CuO[1], Al$_2$O$_3$[1,2], TiO$_2$[2], ITO[2]...	carboxylic acid	−C(O)O−Mt−	−
TiO$_2$[5], Nb$_2$O$_5$[5], Al$_2$O$_3$[5]	phosphoric acid		the SAM structure appears similar to the Au-thiol system, physisorbed species my coexist alongside chemisorbed
activated (−COOH terminated) carbon[3]	amine	−NH−OC(O)−	
graphite and activated carbon electrodes[3]	amine, carboxylic acid, alcohol		the bonding is mediated through further functionalization of the surface, for example with with cyarunate chloride, carbodiimide *etc.*
−OH terminated surfaces: Al$_2$O$_3$ [1], SiO$_2$[1,2], ITO[2], ZnSe[1], Au (with Au$_2$O$_3$ overlayer)[1]...	chloro-, oxy-, amino- silanes	−Si−O−Si−	usually ill-defined, durable but prone to hydrolysis
H−terminated Si[4] (p−doped, n−doped, or intrinsic)	alkene, alkyne	−C−Si−	very durable, deposited by various hydrosilylation techniques, with and without surface functionalization prior to deposition
H−terminated Ge[4]	alkene, alkyne	−C−Ge−	−//−

[1] reviewed by Ulman in 1996[2], [2] reviewed by Smith *et al.* in 2004[3], [3] reviewed by Chaki *et al.* in 2002[4], [4] reviewed by Buriak in 2002 and Yan *et al.* in 2011[5], [5] as reported by Hähner *et al.* in 2001[6]

Self assembled monolayers have been employed in a vast number of various applications such as surface passivation,[7], [8] surface hydrophobization,[9] study of water films,[10] tribology,[11]–[13] patterning, nanolitography, printing,[14]–[16] functionalization of microcantilevers for metal ion sensing,[17], [18] surface modification for biomaterials,[19]–[21] for example drug delivery,[22], [23] bioactivation of implant ceramics for bone binding,[24] modification of teeth and dental materials,[25]–[27] furthermore application of SAMs as a substrate for nucleation and growth of inorganic material crystals,[28] means for the study of lipid membranes,[29] means for the study of electron transfer,[30] immobilization of enzymes and proteins on electrode surfaces for selective biosensing and electrochemical analysis,[4], [31]–[33] molecular photo-devices and photo-sensors,[34] organic electronics,[35]–[37] selective heterogeneous catalyses,[38] preparation of freestanding carbon nanomembranes,[39] preparation of graphene.[40] This is by far not a complete list and more applications were reviewed by Bishop *et al.* in 1996,[41] Tam-Chang *et al.* in 1999,[42] Gooding *et al.* in 2003,[43] Love *et al.* in 2005[44] and Ariga *et al.* in 2008.[45]

Periodic Surface Structures and Their Notation

The notation of adlayer structures is needed for the understanding of literature on SAMs. It is briefly presented here, although not necessary for the understanding of this thesis.

Unreconstructed surface structure of a single crystal is a cut of the crystal through one of its crystallographic planes. Crystallographic planes may be noted by Miller's indices and these, together with the knowledge of parameters of the unit cell of the crystal, provide all the information needed for the virtual reconstruction of the whole surface. Once the unreconstructed surface has been defined, it is possible to use Wood's notation to describe the structures of planar periodic adlayers that have the same symmetry as the original surface. The notation has been established in 1964.[46]

In Wood's notation, a planar primitive unit cell is introduced to allow for a truncation of the surface to the simplest periodically repeating unit which can be identified in an ordered array, the cell is defined by 2 vectors, $\mathbf{a_1}$ and $\mathbf{a_2}$, as seen in **Fig. 1 A** where an example of a face-centered cubic (111) surface and its 2 possible planar primitive unit cells are shown. Periodically ordered surface adlayers are then described by two new vectors, $\mathbf{b_1}$ and $\mathbf{b_2}$ and the structure of the adlayer is noted as $(C_1 \times C_2)R\alpha$, where $C_1 = |\mathbf{b_1}| / |\mathbf{a_1}|$, $C_2 = |\mathbf{b_2}| / |\mathbf{a_2}|$ and α it the angle of rotation between $\mathbf{b_1}$ and $\mathbf{a_1}$, as seen in **Fig. 1 B** where an example of adlayer with $(\sqrt{3} \times \sqrt{3})R30°$ structure is shown. The $(\sqrt{3} \times \sqrt{3})R30°$ structure is common for SAMs of alkanethiols (ATs) on Au(111) surface.
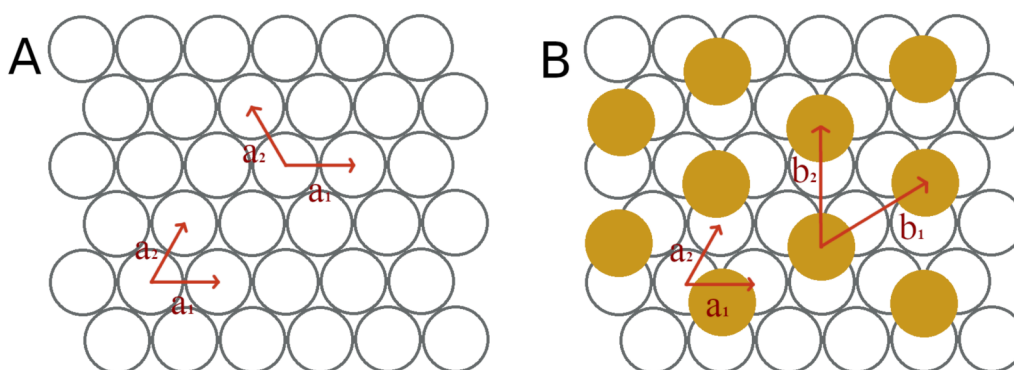

Figure 1: A) Two possible primitive unit cells for fcc(111) surface; B) A (√3x√3)R30° adlayer pattern on fcc(111) substrate.

SAM of Thiols on Gold

Thiol-based SAMs on Au substrate, first reported by Nuzzo *et al*. in 1983 and specially reviewed by a number of authors during the years,[47],[44], [48]–[51] are probably the most often used SAMs for model studies. The Au-thiol system offers an excellent reproducibility for experiments under ambient conditions and being intensively explored, a relatively understood environment for experimentation.

Deposition of the monolayer is done from either a gas phase, usually under ultra high vacuum (UHV) conditions or from a solution. It is usually possible to obtain identical monolayers using thiols and homologous disulfides. Both species give a dense coverage with the molecules standing up and being chemisorbed as thiolates when deposited from a solution.[52] On the other hand, deposition from a gas phase provides additional control over the monolayer formation. Monolayer of a structure identical to the one obtained by deposition from a solution is usually produced with sufficient deposition time under lab. temperature. Monolayers with different structures may be obtained by variation of the deposition conditions. For example a "striped phase" with lower density of molecules and the molecules laying flat on the surface may be obtained by early termination of the deposition. A monolayer with only physisorbed species in their thiol form may be acquired by sufficient cooling during the deposition.[44], [53] It is also possible to obtain different SAM structures for deposition from a solution, by making changes in deposition temperature or by thermal annealing carried out after the deposition.[54], [55]

SAM is a dynamic system which may be noted with the following simplified chemical equilibrium equation: *surface + adsorbate ↔ SAM*. This implies that once the sample is removed from the solution of the adsorbate, the monolayer is thermodynamically unstable. The stability of the monolayer arises from a relatively high activation barrier for desorption, which may be attributed to bonding of the molecules to a surface and to lateral intermolecular interactions within the monolayer. SAMs of ATs usually desorb from the surface at approximately 200 ºC, with the desorption starting at much lower temperatures, for example for octadecanethiol at around 100 ºC.[56]

The thiolate-gold bond enthalpy is approximately 180 kJ/mol,[2] the exact bonding strength depends on the adsorbed specie and on the surface binding site. Possible positioning of sulfur atoms relative to the nearest Au atoms introduce differences of approximately up to ~25 kJ/mol for various binding sites, *i.e.* the difference between two ex-

tremes, the least favorable position, where the S atom is atop of an Au atom and the most favorable position, where the S atom is in a hollow site between 3 Au atoms.[2] It is not yet resolved, what is the exact structure of the thiolate-Au interface for any of the known SAM systems and the aforesaid bond enthalpy difference is obtained merely from a computational study made for an unreconstructed Au(111) surface. A clean Au(111) surface exhibits a (22x√3) "herringbone" reconstruction, leading to an extra density of Au atoms in the surface layer.[57] Deposition of a SAM can lift this reconstruction, while possibly introducing additional surface reconstructions, like ejection of Au adatoms, to accommodate for the demands of the SAM structure and anchoring.[58] Au(111) is the most commonly used Au surface orientation for studies of SAM structures, as it is the thermodynamically preferred orientation. It is important to point out, that different surface orientations may yield different SAM structures, while hosting identical molecules.[59]

Lateral intermolecular forces introduce stabilizing or destabilizing effects, having impact on the final SAM structure. An example are Van der Waals (VdW) forces between aliphatic chains in AT SAMs, where the interaction enthalpy is about 7 kJ/mol per methylene group,[60] thus for long alkyl chains the lateral VdW interactions may yield a strong stabilization. Alkanethiols, like many other thiols with a small molecular backbone, form a hexagonal close-packed structure on the surface, getting as much contact with their neighbors to maximize the interaction enthalpy and simultaneously host as many molecules on the surface as possible. Other packing structures might be enforced through molecular symmetry or through more directional intermolecular interactions, those are discussed later in the text. It's worth noting that differently ordered phases may be also observed for one SAM at different temperatures while exhibiting identical surface density, as observed for hexa(ethylene glycol)-terminated SAMs.[61] Some AT SAMs were also reported to loose their ordering and "melt" with the rising temperature, [62] although not all vibrational and rotational states are accessible for all parts of a molecule as it is still bound to the surface.

SAMs exhibit many defects in their periodic structures just like 3-dimensional crystals. The defects may relate to extrinsic factors, like the flatness of the substrate, deposition method, temperature during and after the deposition, solvent used for the deposition and its purity, and may be optimized to prepare monolayers with lower number of defects and defect types. Some of the defects arise from the fact, that SAMs are non-equilibrium systems unless they are immersed in a solution of the respective adsorbate

and thus are prone to loose molecules over time. Defects in SAMs of thiols on gold were reviewed in 2005 by Love and Vericat.[44], [49]

The surface of a polycrystalline Au film contains inter-grain boundaries, varied representation of different surface orientations, occlusions and crystal twinning, all affecting the structure and the uniformity of the monolayer. Features occurring on both polycrystalline and monocrystalline surfaces are atomic steps or atomic vacancies. Atomic Au vacancies may lead to a reconstruction of the surface during the deposition and subsequently yield vacancy islands, *i.e.* 1 or 2 Au atoms deep depressions in the monolayer. Defects independent on the surface quality are impurities adsorbed on the surface, regions with absent or not well organized molecules and domain boundaries. Some of the defects are shown in F**ig. 2**.
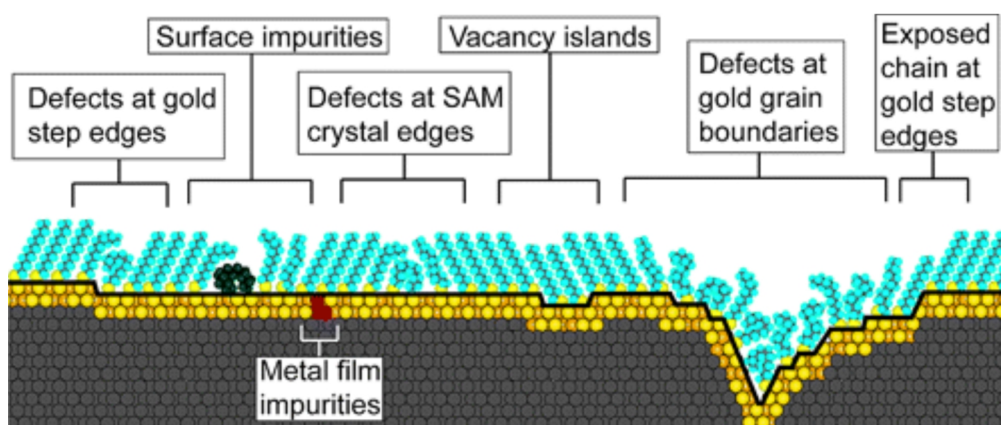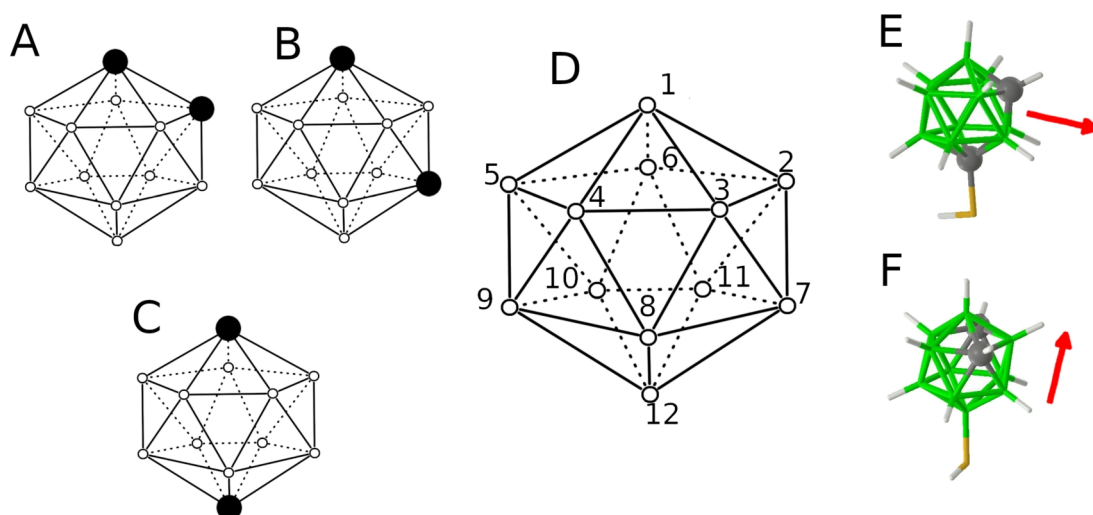

Figure 2: A schematic depiction of some of the defects modeled on an alkanethiol SAM. Taken from the review by Love et al.[44]

Self Assembled Monolayers of Carboranethiols

Thiolated dicarba-*closo*-dodecaborane isomers are thermally and chemically stable molecules suited for self assemblies. The molecules have the geometry close to icosahedral with the dimensions comparable to a rotating benzene ring. Their isomerism offers a number of molecules with different chemical and physical properties while retaining the overall shape of the molecule, giving means to alter the properties of monolayers while retaining the surface pattern. The parental isomers together with the system of notation of the atom positions within a carborane cluster and with some examples of thiolated species are schematically shown in **Fig. 3**.

*Figure 3: **A, B, C)** A schematic depiction of the ortho-, meta- and para- carborane isomers respectively, the boron atoms are represented as blank dots, the carbon atoms as black dots and the hydrogen atoms are omitted for clarity, the full and dashed lines are present only to underline the icosahedral geometry. **D)** The numbering of the carborane cluster vertices. **E and F)** A schematic depiction of the M1 and M9 molecules respectively, with the approximate direction of their dipole moments represented as red arrows.*

The derivatives of carboranethiols were applied to Cu, Ag and Au surfaces, forming self assembled monolayers similar to those of alkanethiols. Carborane derivatives adsorbed or grafted onto other substrates are not discussed here.[63]–[65] Carboranethiols in SAMs obey hexagonal close packing and thus resemble the pacing of solid spheres. The differences between AT and carboranethiol SAMs are as follows. Greater spatial requirements of carborane units over ATs. The nearest neighbor distance (n.n.d.) for unsubstituted carboranethiol isomers on Au substrate is approximately 7.2 Å, the n.n.d. commonly found for plain AT SAMs is about 5.0 Å. The larger n.n.d. might be employed for creation of free volume on the surface, allowing for spatially demanding re-

actions confined to the surface to occur.[66] Carboranethiols offer a greater thermal stability. Chemisorbed AT SAMs start desorbing at temperatures of around 100 ºC, lowering the activation energy need for the desorption through formation of surface bound disulfides. Single alkanethiolate molecules leave the surface at the temperature of about 200 ºC,[67] the temperature at which carboranethiolates desorb from gold surface as well.[68] The spatial separation of sulfur atoms within the carboranethiolate monolayers probably prevents from the disulfide formation. Carboranethiolate SAMs are more resistant to soft X-Ray irradiation than AT SAMs, a feature advantageous for example in long XPS measurements. [69] Importantly, carboranethiol SAMs tend to have less pronounced defects. The defects as observed in STM images are small ~ 1 Å protrusions and depressions, changes in the directionality of molecular rows, *i.e.* rotation domain boundaries, and shifts of the molecular rows, *i.e.* translation domain boundaries, leaving out stacking faults, anti-phase boundaries, twin boundaries, tilt boundaries and vacancy islands that are observed for AT SAM.[70] Defects arising from the substrate surface are of course unaltered.

Some carboranethiols were prepared with the thiol moiety attached to the cluster with a flexible aliphatic link. Those molecules give monolayers with a lower long-distance ordering (smaller domains) but similar packing to carboranes with a thiol group attached directly to any of the cluster vertices.[71], [72]

Molecules adsorbed on metal surfaces alter the surface work function, the effect dependent on the notional dipole moment of the molecules. The change of the work function can be best demonstrated for SAMs of dithiolated 1,2-$(SH)_2$-*ortho*-carborane (O1,2) and 9,12-$(SH)_2$-*ortho*-carborane (O9,12), two isomers with the dipole moments of about 3.7 D and 5.5 D respectively.[73] The two isomers adsorb on the surface in a way that the molecular dipoles are practically perpendicular to the surface but point in opposite directions for the two isomers, for O1,2 the direction of the dipole points towards the surface and it lowers the surface potential, for example of silver by 700 mV, the molecular dipole of O9,12 is pointing away from the surface and rises the surface potential of silver by 300 mV.[74] The two isomers may be also deposited simultaneously to yield a mixed SAM with the work function adjusted in the interval given by the pristine monolayers. The effect of the other isomers is less intensive for their molecular dipoles are either weaker or pointing in a direction which is not perpendicular to the surface.

The molecular dipoles in SAMs of various carborane thiols were utilized also for example to direct the alignment of liquid crystals,[75] or for the creation a model systems for the study of dipole-dipole molecular interactions as discussed in the next section.

Most of the carboranethiol molecules on Au substrates are adsorbed as thiolates and only a minority may be bonded as thiols. The ratio of the thiolate/thiol form of binding has been explored for *para*-carborane derivatives, where the molecules bound as thiols could be removed by heating of the sample.[76] A study of dithiolated species O1,2 and O9,12 shed light on to the nature of the thiol-thiolate binding, showing that more acidic thiols tend to adsorb rather as thiolates and that the thiolate/thiol ratio may be shifted by changes in the acid-base conditions used for deposition or even after deposition, where the latter may be utilized to induce molecular motion on the surface.[77]

SAMs of carboranethiols were also used for protection of metal clusters, namely gold nanoparticles in 2005 by Base *et al.* and gold clusters by Cioran in 2012 and 2014.[68], [78], [79] Carboranethiol SAMs were also analysed for protection of flat silver and copper surfaces, for their superior surface passivation properties.[80], [81]

To mention some more work on carboranethiol adsorbed on gold, the SAMs of M1 and M9 and their mixed SAMs on gold have been characterized by scanning tunneling microscopy (STM) and surface sensitive Fourier Transformation Infrared Spectroscopy (FTIR) by Hohman *et al.* in 2009,[70] those isomers were also characterized by contact angle measurements and ellipsometry and analysed in a computational study by Yavuh *et al.* in 2017,[82] Mete *et al.* did a computational study on various carboranethiols on a flat (111) gold in 2016,[83] Scholz *et al.* published a study on permethylated *para*-carborane on gold in 2011,[72] Some of carboranethiol SAMs have been also reviewed together with adamantanethiols by Hohman *et al.* in 2010.[15] Adamantane is an organic molecule of a diamondoid shape, which has similar spatial requirements as carborane clusters. Its stability on metal surfaces has been proved smaller as the metal-sulfur bonding is weaker in comparison to carboranethiols on gold. This may be observed for example with the relatively easy substitution of the monolayer constituents in a solution of ATs. The substitution is much slower for carboranethiols than for adamantanethiol SAMs.

Lateral Interactions within SAMs

Lateral interactions within self assembled monolayers, like π-π stacking, dipole-dipole interaction, hydrogen bonding, Van der Walls forces, ionic forces and metal-ligand co-ordination are usually somewhat difficult to address, for the structure and stability of a SAM is the result of an interplay of the forces between the substrate and the adsorbed molecules and of all of the interactions between the molecules themselves. This may be well demonstrated with aromatic thiols adsorbed on gold. Aromatic molecules with the thiol group attached through a flexible aliphatic chain tend to form SAMs with a structure similar to aliphatic ATs, that is the commensurate (√3x√3)R30° structure which has been observed for example for benzyl mercaptan or 4-biphenylmethanethiol.[55], [84] Aromatic molecules with the thiol anchor attached directly to the rigid body of the molecule, like for thiophenyl, biphenylthiol or 2-thiophenathrene, form SAMs that either lack any periodic structure at all, the ordered domains are very small or the density of molecules on the surface is reduced.[84]–[87] The difference between the structural patterns for SAMs of flexible and rigid molecules may be assigned to the competition between the π-π stacking of the aromatic cores and the preference of sulfur atoms to bind onto specific biding sites on the surface. An experiment of comparing the structure of chemisorbed thiophenol and benzeneselenol on flat gold surfaces by Kafer *et al.* shows, that the less strongly bound benzeneselenol forms a well ordered long range structure similar to the one of benzene in its crystalline phase and the thiophenol SAM is loosely packed in very small domains,[87] implying that π-π stackings dominates for the less strongly binded benzeneselenol and the sulfur-gold binding sites preference is dominating for thiophenol. Strong π-π interaction has been observed in fluorescence spectroscopy by Reese *et al.* for aromatic structures attached to a gold surface through a flexible aliphatic link.[88]

The dipole-dipole interactions have been usually addressed through introduction of an aromatic system with electron donating or withdrawing substituents. It has been observed by Evans *et al.* that aliphatic ATs with incorporated vertically polarized aromatic groups exhibit altered structures in regard to plain AT SAMs.[89] On the other hand, it is difficult to distinguish whereas the driving force of the change is the introduction of a dipole or of a bulky substituent. Kang *et al.* studied the effects of oppositely aligned dipoles in mixed monolayers, they used ω-substituted biphenyl-4-thiols as molecular dipoles perpendicular to the surface.[90], [91] The observed ratios of the adsorbed SAM

constituents corresponded to the magnitude of the molecular dipoles. Stabilization of monolayers through horizontally aligned dipoles has been explored by Hohman *et al.* in a study of M1 and M9 on flat gold surfaces. The two isomers give identical SAM structures, but their dipoles adsorbed on a surface are almost perpendicular, *i.e.* parallel to the surface for M1 and perpendicular to the surface for M9. The M1 monolayer is more stable compared to its isomeric M9 SAM.[92] Another study from the same laboratory was able to show the orientation of the surface confined dipoles of M1 adsorbed on gold, revealing long distance ordering of the dipoles.[93] A computational study by Mete *et al.* demonstrates that a single M9 molecule binds to Au (111) surface more strongly than a M1 molecule, underlying the dipole-dipole lateral stabilization of the M1 monolayer.[83]

Hydrogen bonding was shown to introduce a strongly directional control over SAM structures. For example ω-carboxylated 3-mercaptopropionic acid adsorbs on gold in a 3 × 3 over-layer structure with a triangular superstructure of trimers stabilized by interactions between the carboxyl groups.[94] SAMs of AT molecules with an internal amide functionality tend to form linear networks with hydrogen bonding as reviewed by Mullen *et al.*[95]

Van der Waals forces were already discussed in the section on AT SAMs on gold.

Metal-ligand and ionic interactions confined to SAMs are promising tools for ion sensing. The advantage of an electrode modified with ω-functionalized SAM is the enhanced sensitivity for electrochemical analysis by selective binding of ions, rising the concentration of the analysed species close to the electrode surface. A relatively novel approach for ion sensing is the use of SAMs adsorbed on a flexible substrate. The subsequent binding of ions onto the monolayer induces lateral stress which leads to macroscopic bending of the substrate. The surface stress may be attributed to the formation of strained intermolecular complexes within a monolayer.[96] Although the sensing methods were studied for a number of metal-ligand systems and substrates as reviewed by Hsu *et al* in 2011,[97] not much work has been directed at the quantification of the observed effects and the density of metal ions adsorbed onto the functionalized surfaces is not often determined or the quantification is inaccurate. The studies of palladium ions adsorbed on a terpyridine-functionalysed Au surface by Poppenberg *et al.* from 2012 illustrate the difficulties encountered.[98], [99] This thesis aims at surpassing this particular gap.

X–ray Photoelectron Spectroscopy

The method is based on the photoelectric effect, the sample is irradiated by high energy electromagnetic (EM) radiation, which is able to excite electrons from their atomic and molecular orbitals (AOs and MOs) to the energy continuum. The electrons ejected from their parental atoms are called photoelectrons (PEs). They travel in all directions inside the sample and are subsequently scattered due to elastic and inelastic collisions, only a part of them leaves the sample. The PEs, once they escape, are focused with electron optics into a hemispherical analyser which, based on their kinetic energies, separates their trajectories through the use of a magnetic field. They then reach a detector which counts their numbers in respect to the position, *i.e.* in respect to the corresponding kinetic energy (KE). A schematic drawing is depicted in **Fig. 4**. The setting of the electron optics defines the acceptance angle, the largest angle in respect to the mean direction from the sample to the analyser under which a relevant number of PEs is still detected.
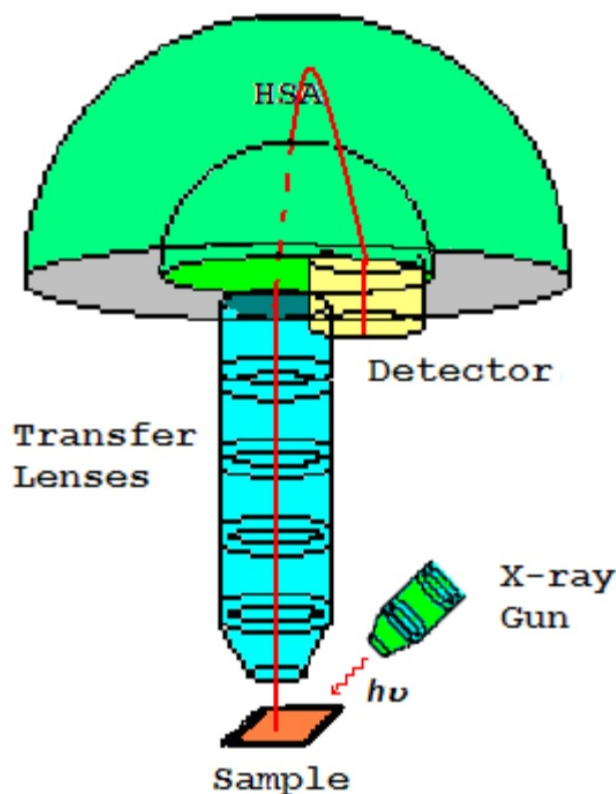

Figure 4: A schematic depiction of a XPS instrument, the picture is taken from the CasaXPS Guidebook. [132]

Each element has a unique set of orbital binding energies (BEs) and although some of the BEs for various elements may overlap, it is possible to identify the elements present in the sample through the detection of the other elemental lines as shown in **Fig. 5**, where a spectrum obtained for the sample of $Tb_2(SO_4)_3 \cdot 8\ H_2O$ is shown. The peaks in the spectrum correspond to PEs emitted from the notated AOs, the peak noted as O KLL corresponds to Auger electrons emitted from oxygen, electrons of this type are discussed later in the text.
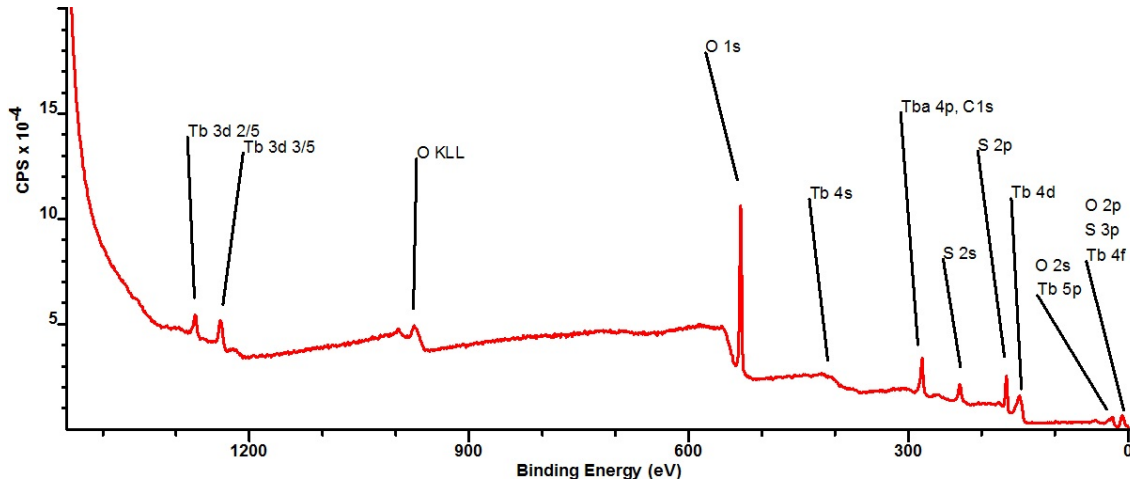
Figure 5: Plot of BE (eV) versus counts of electrons per second (CPS) for the sample of $Tb_2(SO_4)_3$. The signal of Tb 4f, S 3p and O 2p as well as Tb 5p and O 2s or the signal of Tb 4p and C 1s are overlapping and cannot be used alone for the identification of the chemical composition.

The data in the **Fig. 5** are plotted as binding energy (BE) versus CPS. A simple relation is used to convert the KE in to the BE of the detected electrons:

$$BE = h\upsilon - KE - W_s \qquad\qquad (1)$$

where $h\upsilon$ is the energy of the X-ray radiation and W_s is the spectrometer work function, the work function of the sample is not necessary as the Fermi levels of the sample and the analyser are aligned, for they are in electrical contact. This equation gives the BE referenced to the Fermi level. The electrical contact is naturally established only for conductive samples, the energy scale has to be calibrated for insulating samples in order to obtain the correct BEs.

The BE does not represent the orbital energy directly, it is the energy difference between the initial state, *i.e.* before the electron emission, and the final state formed directly after the emission. Both the initial and final states are influenced by the chemical environment experienced by the atoms from which the electrons are emitted, this can be

observed for example for PEs emitted from the S 2p orbital in sulfates in regard to the S 2p electrons from sulfides, the electrons from sulfates are shifted in regard to the latter to higher BE by about + 7 eV.

The distribution of the remaining electrons in the final state is different from the initial state, as the electric field of the nuclei is less shielded since an electron from a core level orbital is missing now. The electrons from orbitals with the quantum number higher than of the emitted electron experience a stronger electric field and consequently their contribution to lowering the over-all energy of the system is greater than in the initial state, rising the measured BE of the emitted PE. The BE can be thus thought of as consisting of the negative energy of the orbital from which the PE is emitted and the relaxation energy attributed to changes in orbital energies after the emission. Theoretical omission of the relaxation energy is called the Koopman's approximation. The relaxation energy always increases the BE and arises due to changes in AOs, MOs and the distribution of charge in the crystal, this means that its magnitude is dependent not only on the particular element, but also on its chemical state. Moreover, the electron left in the half-vacant core orbital has an unpaired spin which interacts with the unpaired spins from the valence sphere, giving rise to signal splitting in case of an open valence state configuration. Additional signal splitting may be observed in spectra of coordination compounds, for the changes in the orbital energies may lead to ligand-to-metal charge transfer, yielding states with and without the transfer. The resulting PE signals, shifted from the line corresponding to the lowest BE to higher BEs, are called the shake-up structures.

Changes in the BE are also introduced in case the material is not conductive and becomes charged due to the emission of PEs. Insulating samples are often neutralized with an electron gun, however, the neutralization of the surface may hardly be quantitative and thus a calibration of the energy scale is necessary. This is usually done by comparison of an elemental line corresponding to a known chemical specie in the obtained spectra with a reference containing the same compound and a calibrated energy scale.

The electron vacancy formed in a core shell orbital after the ejection of an electron is quickly filled with an electron from an orbital with lower BE. The energy difference is usually released in the form of EM radiation, but may be also transferred to another electron, leading to its ejection when the energy is adequate to excite the electron to the energy continuum. Electrons ejected in this manner are called the Auger electrons and their KE is:

$$KE = BE_{core} - BE_1 - BE_2 - W_S \tag{2}$$

where BE_{core} is the binding energy of the primarily ejected electron, BE_1 is the binding energy of the electron filling the inner orbital vacancy and BE_2 is the binding energy of the subsequently ejected electron. The notation of Auger electrons is: the 1st letter denotes the electron shell of the primarily ejected electron, the 2nd letter denotes the electron shell of the electron that filled the vacancy and the 3rd letter stands for the electron shell of the secondarily ejected electron. The KE of Auger electrons is independent of the energy of the used incident radiation.

XPS is a qualitative as well as a quantitative method and the intensities of the measured peaks can be converted in to the relative atomic concentrations. The peak intensity is taken to be the integrated area beneath the peak after a background subtraction. The background comprises of secondary electrons, *i.e.* the electrons which were scattered in elastic and inelastic collisions during their travel through the sample but have escaped the sample. For a homogeneous sample the relative atomic concentration can be simplified as:

$$[Atomic]\% = \frac{n_A}{\sum\limits_A n_A} \cdot 100 = \frac{\dfrac{I_{A_i}}{S_{A_i}}}{\sum\limits_A \dfrac{I_{A_i}}{S_{A_i}}} \cdot 100 \tag{3}$$

where n_A is the molar amount of atoms A in the sample, I_{Ai} is the measured intensity of a peak corresponding to photoelectrons ejected from orbitals of the energy level i of atoms of the element A and S_{Ai} is the relative sensitivity factor (RSF). The RSF is dependent on the spectrometer, the experimental setup, material of the sample, energy of the incident X-ray radiation and the characteristics of the orbitals involved. Terms in the RSF have undergone many changes as for the understanding of their physical background as well as in the nomenclature used since the acknowledgment of the method as

a tool for quantitative analyses in the 1960s, a good care has to be taken not to confuse the terms arising for different models as is discussed later.

The signal intensity I_{Ai} can be broken down as:

$$I_{A_i} = J \, \sigma_{A_i}(h\nu) \cdot \lambda(KE) \cdot Q(KE) \cdot f_{A_i} \cdot M \cdot x_A \cdot T(KE) \cdot K(KE) \qquad (4)$$

where J is the flux of the X-ray radiation, $\sigma_{Ai}(h\nu)$ is the photoionization cross–section for electrons from the particular orbitals and for X-ray radiation of energy $h\nu$, $\lambda(KE)$ is the effective attenuation length and depends on the KE of the PEs and the sample material, $Q(KE)$ is a parameter describing the reduction of photoelectron intensity due to elastic scattering and is dependent on the photoelectron KE, f_{Ai} is the fraction of photoelectrons that are ejected from the corresponding orbitals without the loss of energy due to extrinsic excitation and the term is dependent on the chemical state of the atom, as will be discussed later, M is the atomic density taking in account all the atoms in the sample, x_A is the fraction of atoms of the element A in the sample, $T(KE)$ is the value of photoelectron transmission function for photoelectrons of the given KE, it is dependent upon the experimental setup of the spectrometer and is periodically updated and stored on serviced machines, $K(KE)$ is another term arising from the spectrometer and comprises all the instrument-based factors which are not included in $T(KE)$, it is dependent on the KE of the analysed photoelectrons. The signal intensity as described above is freed of the asymmetry parameter, which takes in to account the anisotropy of photoemission. The asymmetry parameter falls out when the incident X-ray radiation and the mean direction towards the analyser form the so called magic angle of approximately 54,7°. The majority of commercial instruments are installed this way today. The values of $\sigma_{Ai}(h\nu)$ have been calculated by Scofield in 1976 and are used to date,[100] although several new calculations have been made.[101]–[103]

The $T(KE)$ and $K(KE)$ terms arise from the effect of stray magnetic fields, design tolerances, electrons scattered in the analyser, electron-optical transmission of the spectrometer, the efficiency of the electron detection system and the efficiency of the electronic system between the detector and the recording system. The signal intensity is usually divided by the value of the transmission function, $T(KE)$ corresponding to the given photoelectron KE prior to application of the RSF, however, the terms $T(KE)$ and $K(KE)$ are entwined and their exact definition usually lies on the instrument manufacturer. It is unfeasible to use RSFs based on the underlying physics of photoemission when the exact knowledge of both of these functions is not available. An empirically derived RSF lib-

rary is then usually employed. On the other hand, the National Physical Laboratory in the UK offers a commercially available software which is able to compensate for all of the instrument dependent effects by comparison of spectra of selected elements measured on the instrument of interest and the *Metrology Spectrometer II*, a precisely calibrated instrument from the NPL in UK, to yield a calibration function.[104], [105] The obtained calibration function compensates for the instrumental influences, thus spectra obtained and conditioned in this manner are referred to as the true spectra which are comparable between various instruments and manufactures. The use of RSFs based on theory is then feasible. Three types of RSFs are offered by Powell and Jablonski.[106]

The elemental RSF:

$$S_{A_i}^E = \frac{I_{A_i}^{ref}}{x_A^{ref} \cdot I^{std}} \tag{5}$$

where $I_{A_i}^{ref}$ is the signal intensity of photoelectrons from orbitals of the energy level i of the element A in the sample used as the reference, most often pure elements are used as the reference samples, x_A^{ref} is the atomic fraction of the element A in the reference sample and I^{std} is the peak intensity for a selected element and energy level, this elemental line is used as a normalization constant for all RSFs in the given RSF library, usually C 1s or F 1s elemental lines are used. The elemental RSF does not take into account any corrections arising from the measured material.

The atomic RSF:

$$S_{A_i}^A = \left(\frac{M^{std}}{M_A^{ref}} \right) \cdot S_{A_i}^E \tag{6}$$

where M_A^{ref} and M^{std} are the atomic densities of the reference sample and the elemental solid used for the normalization, respectively.

And the average–matrix RSF:

$$S_{A_i}^{av} = \left(\frac{M^{av} \cdot f_{A_i}^{av} \cdot \lambda_{A_i}^{av}}{M^{ref} \cdot f_{A_i}^{ref} \cdot \lambda_{A_i}^{ref}} \right) \cdot S_{A_i}^E \tag{7}$$

where the terms are defined as before, the superscripts *ref* and *av* meaning the reference sample and an average–matrix sample respectively. The values for the average–matrix sample were calculated by Seah *et al.*[107]–[109]

Powell and Jablonski discuss, which RSF type is the one most suited for use. It is possible to calculate the RSF values from their defining equations, the calculation requires knowledge of the elastic and inelastic scattering processes and the processes affecting the final state structure, the first having impact on the way background correction is applied and the latter demanding a separate calculation of f_i for each photoelectron line for every analysed compound.[106] Those requirements are not encountered in databases based on experimental data. Many RSF databases available for commercial XPS instruments are based on the work of Wagner *et al.*,[110] with the original database usually modified to compensate for some of the instrumental effects. Yet this makes the use of XPS very experience-based, the RSFs from the original database of Wagner *et al.* were not obtained from well defined surfaces, *i.e.* the samples were not ion-sputtered to remove the surface contaminants, nor were the data corrected for this contamination, the instrumental terms $T(KE)$ and $K(KE)$ were not well understood, the effect of anisotropy of photoemission was not included in the study and the final state structure effects were not accounted for. Those inaccuracies were of course imported to the new Wagner-based RSF libraries. This problem can be either solved by experience-based changes in the processing of acquired data, *i.e.* the background subtraction as shown in **Fig. 6**, or creation of a custom RSF library based on well defined reference samples. The latter, however, disregards the f_i term again, that is in case when the obtained RSF is used for analysis of different chemical specie different from the reference itself.
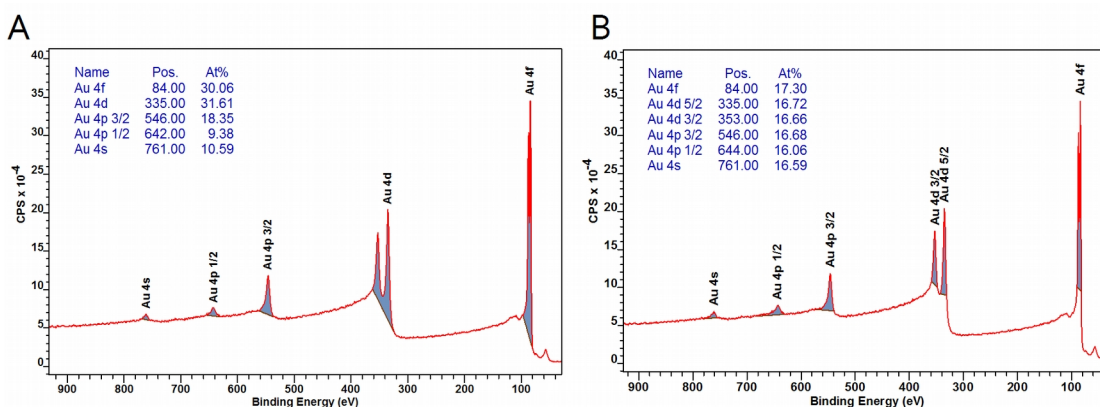
*Figure 6: The spectra of a clean Au surface with the straight line background subtraction method used. Identical way to subtract the background is used for all the PE lines in the **A** spectra. The background subtraction in the **B** spectra is used in a way to obtain approximately identical contribution from all the present PE lines. The blued areas were converted to atomic concentration by the use of equation 3, where the RSFs used were based on the Wagner's database and a correction for the transmission function as provided by the manufacturer was used. The atomic concentrations are shown in the column denoted as At%.*

The mentioned problem of surface contamination is present for samples regardless of their purity. The surface gets quickly contaminated by species adsorbed from its surrounding environment during the preparation of the samples and during the transfer of the sample into the spectrometer. This problem may be bypassed by preparation of fresh sample surface or cleaning of the sample surface under ultra high vacuum (UHV) conditions inside the spectrometer. However, even though the preparation might be done under UHV conditions, the sample surface is still going to get contaminated over time, with the pace depending on the nature of the surface and the vacuum achieved. The exposure of a surface to molecules in a gas phase is described by Langmuir units, $L = 10^{-6} \cdot$ torr $\cdot$ second. The probability of a molecule adsorbing on a surface after collision is relatively low for most surfaces and working in the range of 1 L is often reasonable. The contamination of the surface often comprises of carbonaceous species generally referred to as adventitious carbon. The adventitious carbon signal with the lowest BE is often used as a reference for the spectra, its BE value is 284.8 or 285 eV corresponding to aliphatic carbon.

The soft X–ray radiation usually used, penetrates 1 – 10 micrometers deep into the sample. The electrons ejected in such depths are unable to reach the surface due to electron scattering, limiting the analysis to the order of nanometers below the surface. The photoelectrons which undergo inelastic scattering before leaving the sample are referred to as secondary electrons and are responsible for the background signal in the spectra.

Each inelastic collision deprives electrons of KE and subsequently the KEs of secondary electrons range from their original KE, *i.e.* the KE of electrons as they were emitted from the corresponding AOs, to zero, *i.e.* for electrons which lost all their KE and thus were unable to leave the sample. Elastic scattering also plays a role in the energy loss events, but only indirectly, as it changes the distance traveled through the sample. The acquisition of the theoretical distribution of the secondary electrons in respect to KE is a fairly complex problem which cannot be easily addressed by quantum mechanics due to too many particles involved. Semi-classical models can be employed to resolve the question with a good accuracy as reviewed by Tougaard in 2010.[111] Accurate quantitative analysis is difficult without the knowledge of the distribution, *i.e.* without the knowledge of how to separate the background signal from the signal of primary electrons which didn't undergo inelastic scattering. Models like the straight line method or the Shirley's method which are usually adopted for the background subtraction are not based on the understanding of the physical phenomena and thus limit the analysis to the need of having good reference samples, *i.e.* samples with similar composition and surface structures, otherwise a great deviation from the real value may be introduced as was shown in the **Fig. 6 A**. So far only homogeneous samples were discussed, a method developed for the background separation by Tougaard has been shown to accommodate for the underlying physics and to give results close to the values expected from theoretical predictions for those samples.[112] Samples inhomogeneous in depth pose another problem as can be seen in **Fig. 7**, those are most often addressed through modeling of the expected spectra. To model such spectra requires additional analytical methods or more XPS related experiments, as unknown is not only the chemical composition but also the distribution of elements throughout the surface layers of the sample and the number of variables may become easily overwhelming.
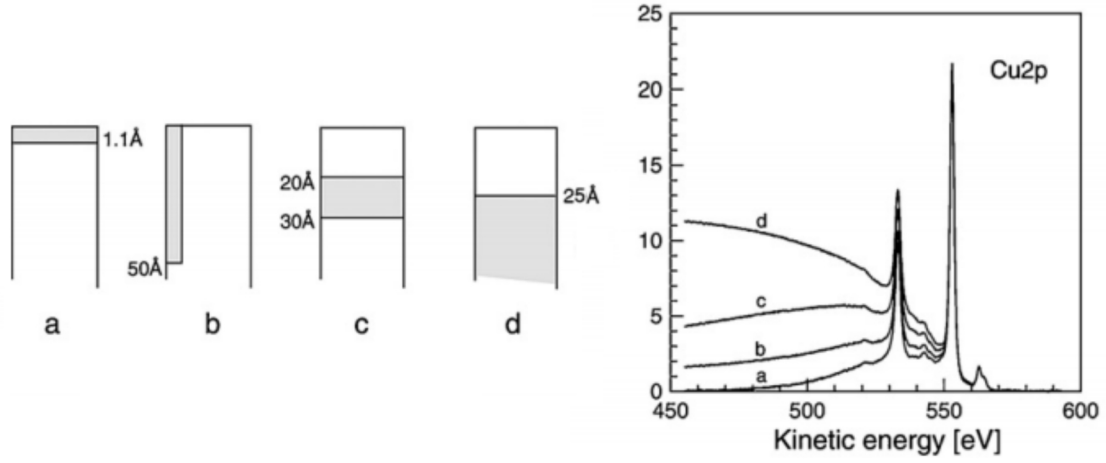
Figure 7: Four different surface and near-surface distributions of Cu atoms (gray) in and on Au, that give identical Cu 2p XPS peak intensities, but quite different inelastic backgrounds as can be seen from the Cu 2p detail spectra on the right. The picture is taken from the article by Tougaard. [111]

The intensity of primary PEs emitted from a sample with an overlaying layer of thickness d obeys the Lambert-Beer's law:

$$I_i = I_i^\infty \cdot e^{\frac{-z}{\lambda \cdot \cos\theta}}$$ (8)

where I_i^∞ is the intensity of PEs originating from AOs of the energy level i, emitted from a sample with practically infinite thickness and without any overlaying material, λ is the effective attenuation length dependent on both the overlaying material and the KE of the PEs and θ is the angle between the mean direction towards the analyser and the surface normal. This relation can be used to obtain the intensity of electrons emitted from a virtual infinitesimally thin layer:

$$\left(\frac{dI}{dz}\right) = I_0 \cdot \frac{-1}{\lambda} \cdot e^{\frac{-z}{\lambda \cdot \cos\theta}}$$ (9)

Consequently the intensity of a homogeneous surface layer of thickness d may be obtained by simple integration:

$$I = \int_d^0 I_0 \cdot \frac{-1}{\lambda} \cdot e^{\frac{-z}{\lambda \cdot \cos\theta}} \cdot dz = I_0 \cdot \left(1 - e^{\frac{-d}{\lambda \cdot \cos\theta}}\right)$$ (10)

Those equations were used by Marel *et al.* to create a calculation method based on EXCEL software with a SOLVER option to provide a means for quantitative analysis of materials with structure composed of homogeneous layers parallel to the surface.[113] The method is described in detail in the above cited article. Marel *et al.* demonstrated the use of the method by determination of the thickness and composition of system based on Si with a SiO_2 over-layer and a carbonaceous surface contamination and of al-kanethiol SAMs on gold. The obtained results were in a good agreement with theoretical predictions and with ellipsometry measurements.

The effective attenuation length used in *equations 4* and *8-10* is based on the average distance an electron with the corresponding KE travels between inelastic collisions and on the prolongation of the overall distance traveled through the medium due to elastic collision. It is defined as:

$$\lambda(KE,d) = IMFP(KE) \cdot Q(KE,d) \tag{11}$$

where *IMFP*(KE) is the inelastic mean free path of an electron with energy KE in a given material and *Q*(*KE, d*) is the term arising from elastic scattering of the electron with energy KE in a given material of thickness *d*. Various models and methods have been developed to predict or to measure the attenuation length of materials.[114]

Concepts, Results and Discussion

Intermolecular bonding *via* Metal Coordination

Monocarboxylated *meta*-carborane thiols 1-COOH-7-SH-*meta*-carborane (M1-COOH) and 1-COOH-9-SH-*meta*-carborane (M9-COOH) are suitable constituents for the formation of intermolecular surface-bound metal coordination complexes. Obeying hexagonal close-packed structure and bearing one metal ion-interacting functional group, the molecules may form complexes with metal cations in the ratio of 1:1, 2:1 or 3:1 as depicted in the **Fig. 8 A, B** and **C** respectively. The combinations of the ratios might be present on the modified surface as schematically shown in **Fig. 8 D**. Defect sites with molecules having pentagonal neighborhood instead of hexagonal can be found in STM images of M1-COOH and M9-COOH SAMs, but those are rather exceptional and rare, and thus without any significant effect on the overall composition. It seemed feasible to direct the attention to only one of the isomers and due to planned work with dicarboxylated 1,7-$(COOH)_2$-9-SH-*meta*-carborane isomer the SAM of M9-COOH was chosen to be used in this study for the subsequent modification by metal cations.
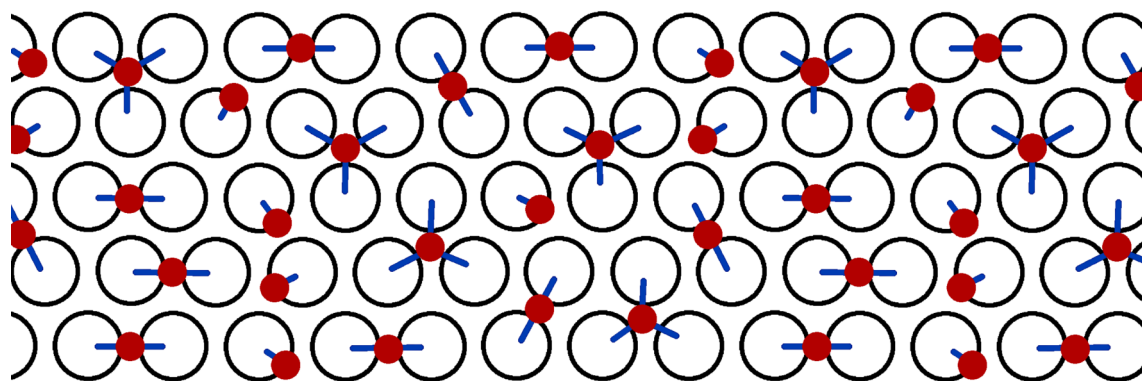
Figure 1: A schematic depiction of the proposed monocarboxylated meta-carborane thiol metal cation coordination complexes formed on a surface viewed from atop. The carborane units are depicted as blank circles, the carboxyl groups as blue lines and the metal cations as red dots. The combinations of 1:1, 2:1 and 3:1 metal to ligand ratios are shown.

A simple geometrical model of the molecules on the surface has been proposed to offer a means to evaluate the possibilities of surface bound carboxyl-cation geometries and so to help with choosing the most promising cations based on their ionic radius and preferred coordination geometry. It proved too many possible conformations and thus

was not used for the cation choosing, however, it is still a useful way to visualize the simplified surface architecture and thus is covered below.

The results of a quantitative XPS analysis based on the Marel's model are presented together with the discussion of their accuracy and then summarized in brief conclusions.

Model of the Surface Geometry

The nearest neighbor distance of both M1-COOH and M9-COOH molecules in their SAMs is estimated from the respective STM images and their evaluation by Fourier transformation as 8.4 ± 0.4 Å.[115] In comparison, the nearest neighbor distance of 1-SH-*meta*-carborane (M1) and 9-SH-*meta*-carborane (M9) in their SAMs has been determined as 7.2 ± 0.4 Å.[93] It has been shown that a carboxyl group attached to the carborane skelet through a carbon apex changes the electron density on the sulfur atom only negligibly,[116] thus the bonding of *m*-carboranethiols and their carboxylated derivatives to Au surface proceeds similarly and the change in the nearest neighbor distance can be attributed solely to either the raise of spatial demands or to introduction of a new lateral intermolecular interaction. The carboxyl moiety introduces the possibility of an orientation dependent hydrogen bonding, yet the changes in the surface structure seem not to bring any anisotropy, *i.e.* the SAM structure seems to be directionally independent. Thus the spatial demands seem more likely to be held responsible. On this basis the molecules were approximated as hard objects without the accommodation of any interactions.

The positioning of the molecules was set periodic in three directions inclining 60º, the sulfur atoms were confined in a plane. The structure of the hardened molecules was derived from the structure of M1-COOH and Van der Waals atom radii. The model aimed at finding the closest packing structures for molecules being arranged both isotropically and anisotropically.

The structure obtained for anisotropic packing of M1-COOH assumes domains with a 38º tilt of the molecules opposite to the direction of the carboxyl group and with the n.n.d. of 7.8 Å in the direction of the tilt, the n.n.d. in the other two directions being 7.4 Å. The surface structure obtained for M9-COOH is assumed to be similar. The tilt angle is measured between the surface normal and an axis of the molecule passing through the sulfur atom and its antipodal boron atom as shown in **Fig. 9 A**. The model for isotropic packing stems from the idea of unhindered molecular rotation around a surface normal,

while the axis of the molecule as defined above is tilted by 13° from the surface normal to minimize the rotating molecule radius. The n.n.d. for this setting was obtained as 8.6 Å, again the model for both M1-COOH and M9-COOH was presumed to be identical.

The model of a SAM with restriction on molecular rotation proves unrealistic when compared with the n.n.d. of 8.4 ± 0.4 Å as observed experimentally in STM, whereas the model with unhindered molecular rotation around the surface normal seems plausible. The largest experimentally validated n.n.d. of 8.8 Å may be accommodated for in a model where the molecular tilt is between 15° and 12°, the molecules with these surface geometries are schematically visualized atop in **Fig. 9 B** and **C** respectively.
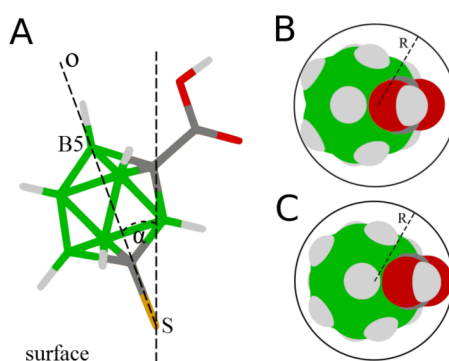
*Figure 2: A) A schematic side view of the modeled conformation of a M1-COOH molecule bonded to gold. The axis of the molecule, **o** is defined as the intersect of the S atom and the antipodal B(5) atom, the molecule is tilted from from the surface normal by angle **α**. B,C) A horizontal projection of the same conformation, with the tilt angle, **α** = 15° and 12° respectively and **R** = 4.4 Å that is for the largest possible n.n.d.*

Carboxyl moiety is able to bind metal cations in various ways, most commonly the metal resides in the plane of the carboxyl group and may be coordinated in a *syn*, *anti* or direct conformation as shown in **Fig. 10**.

Figure 3: A) syn, B) anti, C) direct conformations of carboxyl group and metal cation.

The work of Carrell *et al.* based on crystallographic data processing shows that although this simplified classification may be used as guidance, real systems offer a wide range of O−Mt distances, C−O−Mt angles and out-of-plane deflections when subjected to dif-

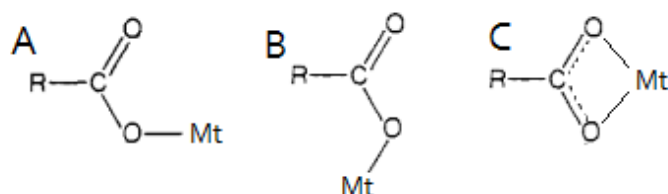ferent carboxylate counter-ions.[117] This implies any geometrical model for the formation of dimers and trimers, as there are too many possibilities. Nevertheless, **Fig. 11** shows a schematic depiction of two molecules facing each other with the nearest neighbor spacing of 8.6 Å, 13° tilt and their carboxyl moieties in plane to give the reader an idea about the surface distances. It is apparent that the variability of the structure of a trimer is greatly enhanced and the tilt of the molecules would be governed by the nature of the cation.
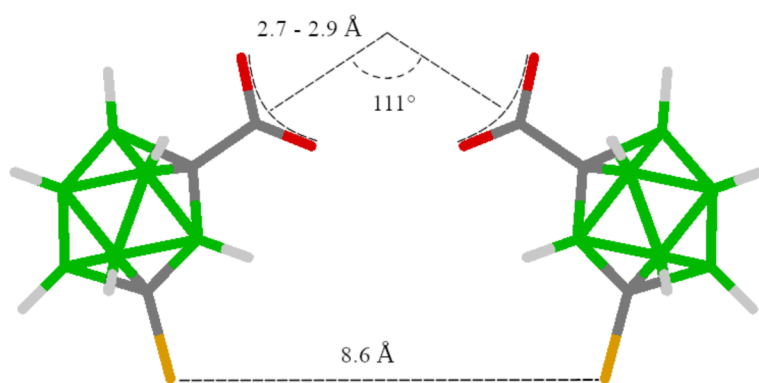
Figure 4: A schematic depiction of two adjacent M1-COOH molecules with 8.6 Å n.n.d. and molecular tilt of 13°. The carbon, oxygen and sulfur atoms are approximately in a plane and the tilt of the two molecules is away from each other.

The the metal cations were chosen on the basis of their XPS PE lines to avoid overlaps with B, C, O, S and Au PE lines. The most stable oxidation states were used, as oxidation-reduction reactions were expected to proceed effortlessly on a surface. The geometrical model was not taken into account when choosing the cations.

X-ray Photoelectron Spectroscopy

The method of Marel *et al.* was used to process the acquired XPS data.[113] Obtained compositions, based on Au 4f, S 2p, O 1s, C 1s, B 1s PE lines and one or two core level PE lines of the particular metal, are presented in **Table 2** together with the derived thicknesses of the layers. The approximations made alongside with other sources of uncertainty are discussed. Other observed phenomenons are presented and discussed together with the metal ions/adsorbed molecules ratios.

The XPS method was tested to prove nondestructive to a SAM of a carborane thiol derivative adsorbed on gold. A monolayer of M9-COOH modified with Ba(II) cation was

analysed for quantitative composition in 1 hour intervals while the sample was unceasingly irradiated by X-ray radiation of power as used for acquisition for 4 hours. No differences were observed in the obtained spectra apart of small scatter of the data by ± 10 %, the scatter was not correlated to a loss of atoms from the surface, neither were observed any changes in the structure of the acquired spectra.

Table 2

TF	Cation	r_{ionic} / Å	Mt:S	Mt:S	B:S	d / Å	D / Å
	plain [Na(I)]	1.0 − 1.4	0.6 (415)	−	11.1	11.5	10.0
	H$_3$O$^+$ [Na(I)]	1.0 − 1.4	0.7 (415)	−	10	8.3	13.4
	Na(I) [6]	1.0 − 1.4	0.3 (415)	0.2 (990)	8.4	13.5	6.6
1	Na(I) [6]	1.0 − 1.4	0.4 (415)	−	8.8	14.0	7.2
	Mg(II) [5,6]	0.6 − 0.9	0.2 (1180)	0.2 (182)	9.0	13.6	5.2
	Mg(II) [5,6]	0.6 − 0.9	0.4 (1180)	0.5 (182)	9.0	13.8	11.8
	Ba(II)	1.4 − 1.6	0.3 (706)	−	8.0	12.5	13.0
	Cr(III)	0.6	−	−	−	−	−
	Ca(II) [2,3,7]	1.0 −1.3	0.6 (1047)	0.7 (291)	13.5	7.5	11.1
	Fe(II) [2,3]	0.6 − 0.9	0.9 (775)	−	10.9	7.6	11.4
	Fe(III) [2,3,4]	0.5 − 0.8	2.3 (775)	−	13.7	7.5	12.6
	Cu(II) [2,3]	0.6 − 0.7	1.1 (554)	−	10.8	8.8	9.9
2	Zn(II) [2,3]	0.6 − 0.9	1.7 (464)	−	13.5	8.2	9.1
	Pb(II) [2,3]	1.0 − 1.5	0.9 (1072)	1.0 (1347)	9.3	8.4	11.6
	Tb(III) [2,3,4]	0.9 − 1.1	1.9 (1335)	1.2 (244) [8]	12.5	8.0	12.5
	La(III) [1,2,3]	1.0 − 1.4	0.7 (650)	−	13.3	8.1	10.4
	Sm(III) [1,2,3]	1.0 − 1.2	2.1 (402)	−	16.7	7.6	10.2
	Ni(II) [1,2,4]	0.6 − 0.7	1.0 (631)	−	7.3	10.7	14.2
3	Sr(II) [1,2]	1.2 − 1.4	0.6 (1353)	−	10.8	18.4	10.9
	Tl(I) [1,2,3]	1.5 − 1.7	0.3 (1369)	−	6.7	17.8	9.1
	Co(II) [1,2,3]	0.6 − 0.9	0.8 (705)	−	8.7	15.1	7.1

The column of "TF" highlights the samples which were measured under identical transmission function and in a separate batch for the preparation of the samples, the "Cation" column depicts the cation used for the monolayer modification, where "plain" refers to unmodified SAM and "H$_3$O$^+$" to a monolayer treated with diluted HCl, both exhibited intrinsic sodium signal. The "r_{ionic}" column refers to ionic radii of the cations, the range of values being given for various coordination numbers,[118] the columns of "Mt:S" are the ratios of metal cation PE signal to the signal of sulfur, with the KE corresponding to the measured PE line of the metal indicated in the parenthesis in eV, the "B:S" column gives the

ratio of the boron PE signal in regard to the signal of sulfur, d and D are the thicknesses of the SAM and the adventitious over-layer respectively, as derived from the multi-layer model;
[1] the raw data were processed with uncorrected RSF of the metal PE lines; [2] the transmission function was not derived properly for this experiment and consequently the obtained results are subjected to a greater error; [3] the thickness of the layers are subjected to a greater error as the signal of Au has been imported from a less precise survey spectrum [4] a sulfate signal originating from the salt used for the SAM modification was present on the surface and was observed in XPS, it's stoichiometry in regard to the thiolate sulfur, that is sulfate:thiolate, is ranging between 0.1 and 0.3; [5] a sodium signal was also observed, however, the concentration of sodium was less than 1/20 in regard to the deposited cation; [6] more experiments were conducted for this setup under identical transmission function, with about 1 month in between the experiments, the results are presented in separate rows; [7] The PE line of Ca 2s as well as Ca LMM are very broad and featureless, however, they are easily extracted from the background, because the background is almost linear in the corresponding region; [8] the signal at 244 eV measured for Tb(III) has been artificially altered to account for an overlap with Au Auger line and thus is subjected to a larger error, which is most likely responsible for the difference between the two PE line intensities; The rows are ordered in way such that the more credible results are positioned higher in the table.

The homogeneity of the distribution of the molecules within a monolayer may play a role in the stoichiometries obtained. A polycrystalline gold surface with root mean square average of the profile height deviations from the mean line of 3.6 Å has been used as the substrate for the SAM deposition. The polycrystalline nature of the substrate might have an effect on the structure of the monolayer formed. The number of molecules that are subjected to substrate grain boundaries in respect to the number of molecules on flat facets can be very roughly approximated in a model of honeycomb lattice with uniform monocrystalline grains that are positioned in a commensurate, not rotated overlaying pattern as:

$$\frac{N_{facet}}{N_{boundary}} \approx C \tag{12}$$

where $C = |\boldsymbol{b}| / |\boldsymbol{a}|$, $\boldsymbol{b}$ is one of the lattice vectors of the overlaying unit cell, that is of the Au facet and $\boldsymbol{a}$ is one of the lattice vectors of the underlaying pattern and its size is the nearest neighbor distance between the adsorbed molecules. The polycrystallinity can then be seen to become negligible only for surfaces composed of larger facets, for example the ratio of molecules experiencing flat surface in regard to molecules confined to a grain boundary is 10 to 1 on a surface with facets of 183 nm^2, when the $n.n.d.$ of 8.4

Å is used. The distribution of the grain size as well as of the crystal orientation was not determined, however, a majority of facets is expected to be (111) oriented and with large facet areas.

Accuracy of the XPS evaluation

The values of the thickness of the monolayers are consistent over the samples with identical transmission functions (TFs).The difference in the thicknesses between the samples with different TFs is not much important in regard to the elemental compositions as is discussed later. It can be seen from those values, how great the TF induced error may be.

Experimental RSF corrections, $C(i)$ were obtained to compensate for the incorrect TFs and unsatisfactory Wagner-based RSFs:

$$RSF_{new}(i) = C(i) \cdot RSF_{Wagner-based}(i) \tag{13}$$

The corrections, based on sulfates with known stoichiometries, give the means of how to obtain the sulfur to metal ratios with better accuracy. The magnitude of the corrections used has been in the range from 0.6 to 1.8. Attempts to obtain corrections for the RSFs of other elemental lines, like B 1s, C 1s and O 1s were not successful due to the difficulty of preparing samples with pure and non-volatile surfaces. Therefore only the cation:sulfur ratios are referenced and the stoichiometries of the other elements are subjected to a greater error, leading to errors in both the thickness of the monolayer and the thickness of the adventitious over-layer, possibly introducing an error of factor up to 2 for the intensity of low KE PEs.

The factor f_{Ai}, defined in the *equation 4* as the fraction of photoelectrons that are ejected from the corresponding orbitals without the loss of energy due to extrinsic excitations, is intrinsically different for the metal ions presented within the SAM and the sulfate reference sample, leading to an error in the composition determination even for data processed with the corrected RSFs. The f_{Ai} factor has been noted to be dependent on the element, the AO and the chemical neighborhood of the emitting atom.[106] Yet the magnitude of the last mentioned source of variation has not been adequately characterized in the literature. It is not expected to be great, based on the author's personal experience.

The multi-layer method developed by Marel *et al.* is based on a model where the distribution of atoms in the layers is homogeneous.[113] The real distribution is, nevertheless, often discrete, as is in the SAM of M9-COOH, where the distribution of atoms in the monolayer obeys the structural motive of the molecules as well as their nearest neighbor spacing. This has such effect, that the Lambert-Beer law as used in the model is only an approximation to the real system, with the accuracy of the model dependent on the atomic homogeneity of the monolayer. This affects the attenuation of electrons from the substrate Au, as the signal then seem as passing through an apprently thinner homogeneous over-layer. This leads to exaggeration of PEs with higher KEs over the ones with lower KEs emitted from the over-layer in respect to the real thickness. Atomic concentrations deduced from a signal of PEs with high KE might thus appear larger than atomic concentrations based on PE of lower KE. A simple example of this problem can be thought of as a surface obstructed with discs with a diameter of 7.4 Å that are arranged with the 8.6 nearest neighbor spacing, *i.e.* about 67 % of the electrons escaping only in the direction of the surface normal from the substrate is attenuated and the rest passes without change which leads to an increase of the apparent disc height by about 25 % in comparison to a homogeneous monolayer with the thickness of 10 Å. The difference in the thickness which is used in the *equation 10* for the computation of the stoichiometry of elements in the SAM has a visible effect only for signals of electrons with very low KE (bout 200 eV and lower), where the change can be seen on the first decimal place. The difference becomes quickly negligible for electrons with higher KEs. Moreover, the scatter of thickness values of modified SAMs as seen in **Table 2**, which is probably introduced through imprecise transmission function in the region of Au 4f (1402 eV), is of greater magnitude than the one just discussed. The observed thickness differences do not impose a big effect on most of the stoichiometries, for example the change of thickness d from 15 to 8 Å in SAM modified with Co(II) leads to a decrease by 5 % in the apparent cobalt content in the monolayer (determination of cobalt by Co 2p PEs with KE of 705 eV). A greater difference can be seen for a monolayer modified with Mg^{2+} (determination of magnesium by Mg 1s PEs with KE of 182 eV), the change of the monolayer thickness from 13 to 8 Å leads to a decrease of the Mg content by almost 20 %. Yet the magnesium content based on Mg KLL Auger electrons (1180 eV) remains constant after the change, *i.e.* because the KE of Mg KLL is quite similar to the KEs of B 1s (1297 eV), S 2p (1325 eV), C 1s (1201 eV), the main components of the monolayer.

The uncertainty of the exact SAM structure and the inhomogeneous distribution of atoms within the monolayer doesn't enable to separate parts of the SAM into distinguishable layers, which would be beneficial, as the position of metal cations is expected to be in the upper half of the monolayer and the model used, *i.e.* the model in which atoms are distributed homogeneously within the layer, overstates the species located closer to the surface in the real system. However, the exact position and thickness of the virtual layers, is not accessible with enough accuracy and so the correction for signal attenuation by additionally separated over-layers was not used. Thus the concentration of boron appears slightly lower in relation to the concentration of metal ions, the concentration of sulfur atoms has been accommodated for in the same way as in the work of Marel *et. al.*,[113]:

$$I_{Sulfur} = I_0 \cdot \left(e^{\frac{-d}{\lambda \cdot \cos\theta}} - e^{-2\frac{d}{\lambda \cdot \cos\theta}} \right) \tag{14}$$

This adjustment makes the apparent sulfur concentration slightly overestimated, yet this overestimation of both metal cations and sulfur is negligible compared to the inaccuracy of the method introduced by the use of incorrect transmission function and RSFs.

Reaction of the monolayer to acidic conditions

The samples measured under identical conditions of the spectrometer, that is samples marked under the same TF, embody comparable thickness values of the monolayer. This trend is broken only for the sample of Zn(II), for which the Au 4f signal has been obtained differently from the other samples in the group, and for samples treated with diluted acid. The lower thickness of the samples exposed to acidic conditions is attributed to partial desorption of the monolayer and has been verified for SAMs of M9 and 1-COOH-12-SH-*para*-carborane (P1-COOH) as can be seen in **Table 3**.

Table 3

SAM	d of pristine SAM / Å	d of SAM treated with acid / Å
M9	10.5	9.2
M9-COOH	11.5	8.3
P1-COOH	13.1	7.1

The thickness d of pristine SAMs and the identical *SAM*s treated with diluted hydrochloric acid. All the data has been acquired under identical instrumental setting.

The acid-base reaction of the monolayers is puzzling because although the thiolate moiety clearly responds to the changed conditions, the carboxyl group seems to be unaffected, as the ratio of sodium to sulfur is not decreased, on the contrary, it is increased after the acid treatment, as recapitulated in **Table 4**.

Table 4

Sample	Mt:S	Au:S	Au:Mt	d / Å
M9-COOH	0.6	74.9	44.34	11.5
M9-COOH + H_3O^+	0.7	88.5	48.3	8.3
M9-COOH + NaCl	0.4	50.5	48.1	14.0

The metal to sulfur ratios, gold to metal ratios and monolayer thicknesses of pristine M9-COOH SAM and identical monolayers treated with diluted HCl or aqueous NaCl solution, all the samples were measured on the same day. The metal to sulfur ratios are based on the intensity of Na 1s PE line at 415 eV and S 2p PE lines at 1324 eV and were processed with the Marel *et al.*'s model, the ratios with gold are based on he intensity of Au 4f PE lines at 1403 eV, Na 1s PE line and S 2p PE lines and only a correction for adventitious adlayer was used.

Bare gold has been treated with aqueous solutions of EtOH, NaCl and $BaCl_2$ in the same way as the adsorbed monolayers to characterize the affinity of the ions to unmodified Au surface. The resulting sodium and barium contents related to Au signal in respect to the samples with adsorbed monolayers were ~ 15 %, ~ 7 % and < 5% of the same ion present within the monolayers respectively. No over-layer correction for the bare gold samples as well as for the samples with monolayers was used for the above mentioned percentage, this should not make much difference in case the ions are located mainly in the upper parts of the monolayer. This means that the ratio of ions to sulfur should be lowered upon desorption of the M9-COOH monolayer, *i.e.* in case the adsorption sites formerly occupied with the constituents of the monolayer and consequently freed due to the acidic conditions are equivalent in the affinity of ions to unmodified Au surface. The freed sites may actually be prone to enhanced adsorption of ions due to surface reconstruction of the substrate, this study unfortunately offers no means to account for such process.

The unexpected response of the system to acidic conditions may be explained through spatial demands or electrostatic repulsion of the surface bound ions, *i.e.* the lowering of the density of carboxylated molecules alias binding sites for the metal ions on the carboxyl-functionalised surface may lead to more favorable binding between the ions

and the carboxyl groups. This is supported by the observation that the sodium content in relation to Au signal remains approximately constant after the partial desorption of the monolayer, which may be observed in the Au:Mt and Au:S ratios in **Table 4**.

The ratios obtained for the unmodified M9-COOH SAMs in regard to the monolayers modified with a solution of NaCl has not been adequately rationalized.

One of the possible explanations may be the solvent effects. The monolayers were deposited from 96% ethanol solutions and the cations were deposited from aqueous solutions. The plain M9-COOH SAM was not treated with water to account for this difference and thus makes the difference in the structure of the monolayer possible. The accuracy of the instrument is less likely to be the cause, for reproducibility of the measurements were not a concern based on previous work done on the instrument by the author.

Metal to sulfur ratios

The pristine M9-COOH SAM as well as the M9-COOH SAM exposed to acidic conditions contained sodium ions on the surface and all of the cations, except for Cr(III), proved to displace the sodium ions quantitatively. No ion exchange was observed for the Cr(III) specie.

SAMs of pristine M9 and of M9 subsequently exposed to a source of Na(I) ions in the same way as M9-COOH SAM samples were analysed for sodium on the surface. The presence of sodium implies that the metal ions may be trapped on the gold-sulfur interface. No traces of sodium were observed on the surface of the samples lacking carboxyl groups.

The behavior of the carboxylate moiety makes it difficult to decide whether the carboxyl groups are present in their protonated or deprotonated forms and consequently if the measured ratios of sulfur to cation, alias adsorbed molecules to cation, reflect the formation of intermolecular complexes on the surface or simply the affinity of the surface bound carboxyl groups to the particular cation in regard to their affinity to a proton or whereas the spatial demands of cations or electrostatic repulsion between carboxylate groups or cations are the driving forces.

The low correlation between the ionic radii accessible for the cations and their surface concentration in regard to the concentration of the adsorbed molecules make the spatial demands less likely to be a ruling factor. The other effects may be subjected to various hypothesis based on the obtained data. It would be unwise to draw any generalizing

conclusions without additional experimental work focused on the comparison of more similar systems in which the number of differences, *i.e.* unknown factors, is smaller.

This study can be thus viewed as laying the first necessary basis for more detailed future work, pointing at interesting directions. For example a study which would utilize the obtained cation:carborane unit ratios to be explored with a surface imagining technique, or a study to explore the cation:carborane ratio in respect to the oxidation number of the same element, as can be seen for SAMs modified with Fe(II) and Fe(III) species. The detailed Fe 2p spectra of both monolayers show slightly different features and it is thus expected that iron is indeed bound in different states in those samples and no quantitative oxidation or reduction occurred upon adsorption of the cations on the surface from the solutions.

Dipole-dipole interaction

Isomers of dithiolated *o*-carborane, 1,2-(SH)₂-*ortho*-carborane (O1,2) and 9,12-(SH)₂-*ortho*-carborane (O9,12) possess relatively large dipole moments, calculated as 3.7 D and 5.5 D respectively.[73] Both isomers form SAMs with identical packing and 7.6 ± 0.5 Å nearest neighbor spacing, with their dipoles being approximately normal to the surface[77]. The dipoles of O1,2 and O9,12 adsorbed on a surface point in the opposite directions, which makes them excellent constituents for the study of dipole-dipole interactions within SAMs. The molecules as adsorbed on the surface together with their dipole moments are schematically depicted in **figure 12**.
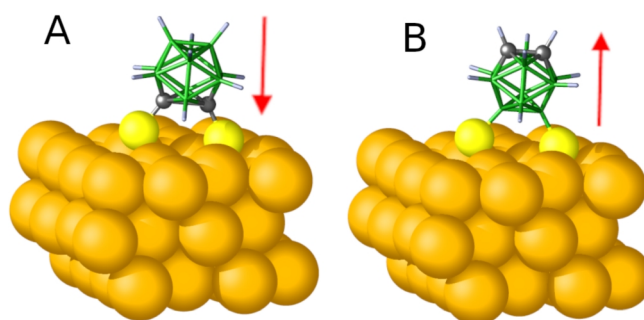
Figure 5: Oppositely adsorbed molecular dipoles of A) O1,2 and B) O9,12 on gold. The carbon vertices are marked as gray.

Dipole-dipole interaction is a long range interaction, the adsorbed molecule doesn't interact only with the nearest molecules but also with the more distant ones. It is possible to calculate the interaction enthalpy per molecular dipole of such a system. It is important to note that the molecular dipole represents only an approximation of the electron density distribution within the molecule.

The interaction enthalpy for densely packed dipoles in SAMs of pristine O1,2 and O9,12 as well as in the mixed SAMs of both isomers with their mutual ratios of 1:1 and 2:1 (surface concentrations) were calculated in this study as 22 kJ/mol, 48 kJ/mol, −4 kJ/mol and −2 kJ/mol respectively. The small interaction enthalpy for the mixed SAMs demonstrates that the dipole−dipole interaction does not offer much help for the formation of the monolayer in respect to a free Au surface. On the other hand, the decrease in the interaction enthalpy for mixed SAMs in respect to the pristine O1,2 or O9,12 monolayers is non-negligible.

The difference in stability of the mixed monolayers and the pristine SAMs of O1,2 and O9,12 might be possibly observed in Thermal Desorption Spectroscopy. Visualization of the distribution of the dipole carriers within the mixed SAMs might be also possible, that is through marking of one of the isomers after deposition prior to an STM analysis. The O9,12 isomer adsorbed on a metal substrate has the carbon vertices facing away from the substrate. The exposed C vertices might be utilized for after-deposition modifications as is discussed bellow. Another method for visualization of the distribution might be through the comparison of simultaneously acquired maps of surface topography and local barrier heights, as has been done for visualization of lateral molecular dipoles in M1 and M9 isomers assembled on Au.[93] The lateral distribution of the isomers within a monolayer and methods for their selective modification is of interest particularly for spatially favorable immobilization of enzymes on an electrode surface, that is without the loss of their function.[119]

Attempts to modify O9,12 monolayers had been done *via* metallation-based reactions. The goal was to introduce carboxyl groups or alkyl chains on to the surface as schematically shown in **Fig. 13**.

XPS analysis of the obtained products shown that the resultant surfaces were contaminated with undesired chemical species. Contact angle measurements gave more promising results, the samples used for carboxylation became more hydrophilic and the alkylated ones were more hydrophobic than the parental surface. Nevertheless, the concept of modification of the surface confined molecules was left out from the scope of this study.
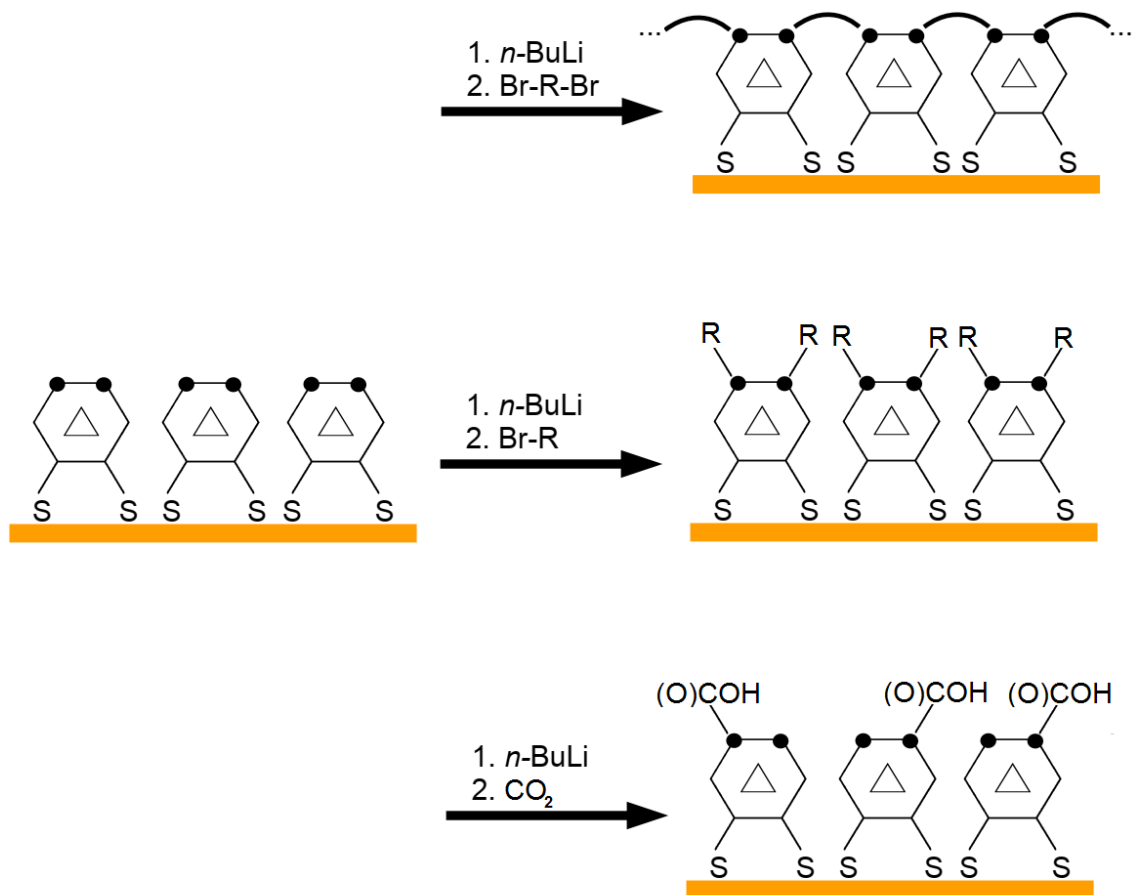
Figure 6: A schematic depiction of O9,12 monolayer on gold is depicted on the left and a schematic depiction of the desired products is on the right. All the experiments begin with the lithiation of the monolayer with n-butyllithium, followed by the introduction of dibromoalkane, bromoalkane or CO₂ reagents.

Conclusions

A literature survey applicable as an introduction to the field of SAMs has been presented. Formation of intermolecular metal coordination complexes within a SAM of M9-COOH has been proposed and presented together with a simple geometrical model of carboxylated *meta*-carboranethiol molecules confined to a surface.

Formation of metal coordination complexes within the monolayer of M9-COOH has been addressed and analysed with XPS for 17 metal ions. Corrections for RSFs were acquired experimentally and the method for determination of multi-layer composition elaborated by Marel *et al.* was used to obtain quantitative information on the surface composition.[113] The sources of uncertainty in the obtained XPS data were discussed. Quantitative composition was determined for three sets of samples. One of the sets was analysed in a way which eliminates most of the error sources.

The metal ion/M9-COOH surfactant ratios obtained from the XPS analysis for Na(I), Mg(II), Ca(II), Sr(II), Ba(II), La(III) and Tl(I) species evidence for the possible intermolecular coordination complex formation within the adsorbed monolayers. On the other hand, unexpected response of the M9-COOH monolayer to acidic conditions was observed. The acidification led to a partial desorption of the monolayer and did not seem to have a decreasing effect on the metal ion/M9-COOH ratio. This means that the observed ratios alone do not provide a convincing evidence on the formation of intermolecular complexes as was expected. A combination of the measured XPS data with results from other surface sensitive techniques such as STM and ToF-SIMS, which is beyond the range and scope of this thesis, might provide a comprehensive picture of metal ions binding to the ω-carboxylated SAMs. From this point of view this thesis provides the first necessary step towards that goal but also represents a limited view on this complex issue.

Sodium ions were intrinsically present on the M9-COOH modified surface, originating from the surrounding environment. The other metal ions, which were experimentally introduced, showed successful in displacement of the naturally occurring sodium ions. The displacement was not always quantitative, as demonstrated with Mg^{2+} ions. The solution of $Cr_2(SO_4)_3$ did not have any proven effect on the monolayer and chromium(III) was the only specie which did not adsorb on the surface at all. Iron in both common oxidation states, *i.e.* iron(II) and iron(III), has been deposited on M9-COOH

modified surface. The iron content within the modified monolayers was largely different between the two species. This observation implies that a metal ion adsorbed on the carboxyl-functionalized surface does not undergo oxidation/reduction reactions on its own easily.

Dipole-dipole stabilization of a mixed SAM of O1,2 and O9,12 isomers was proposed together with the means to determine the ratio and spatial distribution of O1,2 and O9,12 molecules on the surface *via* surface confined chemical reactions followed by XPS and STM analyses. Experiments on a pristine O9,12 monolayer proved the adsorbed monolayer to be very sensitive to reaction conditions. Further experiments on the aforementioned mixed SAM were left out of the scope of this study.

Methods

Chemicals

Diethyl ether was refluxed over sodium with benzophenon until blue or dark purple in color and then distilled under Ar, ethanol 96% p.a. was used as purchased from Lachner, ethanol absolute p.a. was used as received from Penta, HCl 35% p.a. was used received from Lachner, 9,12-$(SH)_2$-*ortho*-carborane was purified by repetitive crystallization from pentane with chloroform, the purity of 9,12-$(SH)_2$-*ortho*-carborane, 1,2-$(SH)_2$-*ortho*-carborane and 9-SH-*meta*-carborane used was confirmed by ^{11}B and ^{1}H NMR spectroscopy, *n*-butyllithium solution 2.5 M in hexanes was used as received from Sigma-Aldrich, 1-bromoctane of >98 % purity was used as received from Fluka, 1,3-dibromopropane of >98 % purity was used as received from Merc, NaOH p.a. was used as received from Penta, the container with NaOH pelets was opened a long time ago and thus the water content was not negligible, crystalline $Na_2SO_4 \cdot x\ H_2O$ of white color was used as received from Lachema, crystalline $Cr_2(SO_4)_3 \cdot x\ H_2O$ of dark green color was used without purity affirmation, crystalline $FeSO_4 \cdot 7\ H_2O$ p.a. of blue-green color was used as received from Penta, crystalline exsiccated $Fe_2(SO_4)_3 \cdot x\ H_2O$ p.a. of yellow-brown color was used as received from Riedel-de Häen, deliquescent $Co(NO_3)_2 \cdot x\ H_2O$ p.a. of brick red color was used without purity affiramtion, deliquescent $Ni(NO_3)_2 \cdot 6\ H_2O$ of transparent green color was used without purity affirmation, crystalline $NiSO_4 \cdot 7\ H_2O$ p.a. of green color was used as received from Chemapol, crystalline $CuSO_4 \cdot 5\ H_2O$ of blue color was used without purity affirmation, $ZnSO_4 \cdot 7\ H_2O$ of 99.995 % trace metal basis purity was used as received from Sigma Aldrich, crystalline $Pb(NO_3)_2$ p.a. of white color was used as received from Lachner, $PbSO_4$ of 99.995 % trace metal basis purity was used as received from Sigma Aldrich, anhydrous $MgSO_4$ p.a. was used as received from Penta, $CaCl_2 \cdot x\ H_2O$ of white color was used without purity affirmation, $CaSO_4$ of 99.993 % trace metal basis purity was used as received from Alfa Aesar, crystalline $SrCl_2 \cdot x\ H_2O$ of white color was used without purity affirmation, $BaSO_4$ of 99.998 % trace metal basis purity was used as received from Sigma Aldrich, $La_2(SO_4)_3 \cdot x\ H_2O$ of 99.99 % trace metal basis purity was used as received from Sigma Aldrich, $Sm_2(SO_4)_3 \cdot x\ H_2O$ of 99.9 % trace metal basis purity was used as received from Sigma Aldrich, $Tb_2(SO_4)_3 \cdot x\ H_2O$ of 99.9 % trace metal basis purity was used as received from Sigma Aldrich.

Synthesis of 1–COOH–9–SH–1,7–dicarba–closo–dodecaborane

The M9-COOH isomer was synthesized according to the literature.[116]

Deposition of the monolayers

Platypus Temple-Stripped Gold Chips were used as the substrate for all the experiments. The Platypus chips were cleaved just before use to minimize their exposure to air.

For the deposition of *meta*-carborane derivatives, the substrate was immersed in to a 96% ethanol solution (from 1 to 4 mmol · dm^{-3}) of the corresponding carborane compound for 50 to 70 minutes, then rinsed with 96% ethanol and dried in a stream of argon or nitrogen. The samples were then stored under inert atmosphere and subsequently used for further modification or measurements within the next 30 minutes. Absolute ethanol was used as the solvent for the preparation of samples subsequently modified with Ni(II) ions.

For the deposition of 9,12-(SH)$_2$-*ortho*-carborane, the substrate was immersed in to a 96% ethanol solution (from 0.5 to 1 mmol · dm^{-3}) of O9,12 with 2.2 molar equivalent of NaOH for 50 to 70 minutes, then rinsed with 96% ethanol and dried in a stream of argon or nitrogen. The samples were then stored under inert atmosphere and immediately used for further modification. The same procedure was tested with deposition on sputtered gold film on glass wafer, but the film started to peel off.

It is important to note, that the ethanolic solutions of the used carboranethiol derivatives were prone to turn opaque several hours after their preparation, thus fresh solutions had to be prepared every time.

Introduction of metal coordination centers to the M9-COOH monolayer

The samples with deposited SAM were immersed in to an aqueous solution of the corresponding salt of 7 ± 3 mmol · dm^{-3} concentration, that is for NaCl, MgSO$_4$, CaCl$_2$, SrCl$_2$, BaCl$_2$, Pb(NO$_3$)$_2$, Fe$_2$(SO$_4$)$_3$, Ni(NO$_3$)$_2$, Co(NO$_3$)$_2$, CuSO$_4$, ZnSO$_4$, La$_2$(SO$_4$)$_3$, Sm$_2$(SO$_4$)$_3$ and Tb$_2$(SO$_4$)$_3$. The FeSO$_4$ and Cr$_2$(SO$_4$)$_3$ were deposited from acidified aqueous solutions with 2.8 μmol · dm^{-3} and 28 μmol · dm^{-3} H$_3$O$^+$ ion concentration respectively. The solution of Cr$_2$(SO$_4$)$_3$ was prepared by boiling of the sulfate in acidified distilled water for 1 hour. All the solutions but that of Na$_2$SO$_4$, FeSO$_4$, Fe$_2$(SO$_4$)$_3$ and MgSO$_4$ were generally prepared two days in advance. The samples were immersed into

the solutions for 50 to 70 minutes, then rinsed with 96% ethanol and dried with argon or nitrogen and stored under inert atmosphere until analysed, that is for 30 minutes at most.

Modification of the O9,12 monolayer

Handling of the reactants was done with care to avoid contact with air, syringes with needles and rubber septa were used for the transport of solvent and reactants. The reactions were done in an installation as depicted on **Fig. 14**, which was mounted from preheated pieces. A sample modified with O9,12 was placed on the fritted glass C while the installation was still warm and it was flushed for several minutes with Ar from valve A to valve B and with a needle penetrating septum D. The needle was then removed and the valves were closed. All the reagents were added through septum D with a simultaneously inserted needle to minimize the over-pressure. About 40 ml of diethyl ether were added first, it stayed above the fritted glass C and bubbled for the whole duration of the experiment. N-butyllithium, 0.5 ml was added drop wise over about 5 minutes and the reaction was allowed to bubble for the next 8 minutes. A stream of diethyl ether was introduced through septum D and the valve B was opened to flush. The sample was washed with ether and then the valves were closed to submerge the sample again. Samples prepared in this manner were then used for subsequent modification. The following scenarios were: **A**) Two drops of 1,3-dibromopropane were added and the mixture was allowed to bubble for 20 minutes. **B**) 1-Bromoctane, 0.13 g was added dissolved in 5 ml of ether. **C**) A source of CO_2 from dry ice was connected to valve B and the valves A and B were opened simultaneously, CO_2 was allowed to bubble through for about 20 minutes. The samples were then flushed with ether and dried in Ar and stored under inert atmosphere until analysed, *i.e.* in 1 day for the contact angle measurements and in about a week for the XPS measurements.
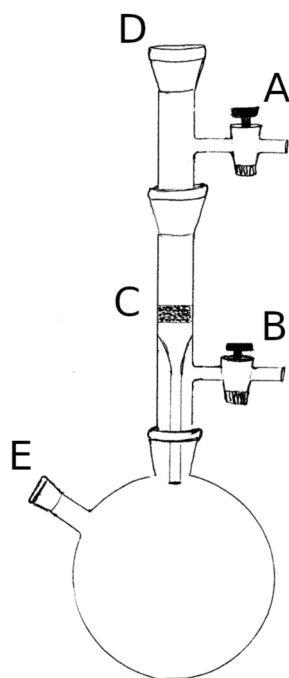

Figure 1: A) Valve; B) valve; C) fritted glass; D) rubber septum E) rubber septum

Determination of the $C(i)$ parameter in *equation 13* for correction of RSFs for metal PE lines in regard to S 2p line

The sulfates were freshly ground to fine dust, stick on a double side conductive sticky tape, blown over with a stream of nitrogen and immediately transferred to vacuum chamber in the spectrometer. Some of the samples underwent partial loss of hydrate water when under vacuum, this has been observed through the change of color. The samples were measured as described in the next item. The measured PE intensities were corrected with the Marel *et al.* model for an over-layer of adventitious carbon and oxygen and the $C(i)$ parameters for the metal RSFs were generated to account for the correct metal to sulfur ratios.

X–ray photoelectron spectroscopy

XPS analysis was performed on a XPS Kratos Axis Supra instrument, using ESCApe software. Aluminum anode with 15 mA emission current was used, charge compensation electron gun was used with filament current of 0.43 A, filament bias of 1.05 V and charge balance of 4.6 V for all the samples but bare gold, for which the electron gun was turned off. The charge compensation was, however, not necessary for the SAM samples as they behaved as conductors. The hybrid lenses and a slot or 110 μm apertures were used in electron optics, giving the acceptance angle of about 20º. The analysis was done under vacuum of 10^{-8} to 10^{-9} torr, the measurements of reference samples of freshly powdered sulfates were done under less favorable vacuum, but not dropping under 10^{-7} torr.

The spectra were processed in CasaXPS software. The Shirley-type background was used for the reference sulfate samples and Au 4f PE lines for all the samples, the linear-type background was used for all the PE lines but the Au 4f PE line in the SAM samples and bare gold samples. The RSFs supplied in Kratos Axis library were used for all the PE lines but the ones mentioned in the **Table 2**, those were derived from the reference samples.

The Marel *et al.* model

The model was implemented to EXCEL software and used as described in the work of Marel *et al.*[113] For SAMs, the Au 4f PE lines were assigned to the substrate, the S 2p and B 1s PE lines and the PE lines corresponding to the deposited metal ions were as-

signed to the monolayer, the C 1s and O 1s PE lines were divided to give the correct carbon and oxygen content in the monolayer, that is 3 parts of carbon and 2 parts of oxygen to 10 parts of boron and the rest was assigned to an adventitious over-layer. For sulfates, the S 2p PE lines and the metal PE lines were assigned to the substrate together with a stoichiometric ratio of oxygen, the rest of the O 1s PE intensity was assigned to an adventitious over-layer together with C 1s PE line intensity. The oxygen present in the form of water hydrate was not taken into account, for its content after the dehydration induced under vacuum was uncertain. This probably led to a slight overestimation of the amount of oxygen present within the adventitious over-layer, making it's apparent thickness larger.

The effective attenuation length (EAL) values used in the multi-layer method were obtained from the NIST Electron Effective-Attenuation-Length Database software.[120] They proved to give results differing only by up to 10 % in the determination of chemical composition of the monolayer and by 5 % in the determination of the monolayer thickness when compared with results obtained for data to which the inelastic mean free path (IMFP) was applied instead of EAL. The IMFP values were obtained from the NIST Electron Inelastic-Mean-Free-Path Database software.[121] Consequently IMFPs were used in place of EALs, with regards to the uncertainty of correct density of the monolayer and it's band-gap energy.

The TPP-2M equation in the NIST Electron Inelastic-Mean-Free-Path Database was used to calculate the IMFP values. The equation was screened for changes induced by the input data, *i.e.* the band-gap energy, density of the material, number of valence electrons of the atoms and chemical composition. All the input was chosen to test the extreme values obtained by earlier calculations of the IMFPs and the resulting compositions obtained from the Marel's method for quantitative analysis of SAMs modified with Na(I), Fe(II), Fe(III) and Pb(II). The results yielded differences no larger than 10 % in the monolayer thickness as well as its composition in comparison to the primary calculation. Consequently the original input was used for all of the SAMs regardless of their composition, that is $\rho = 0.8$ g $\cdot$ cm^{-3}, *band-gap energy* = 5.6 eV, stoichiometry: $H_{10}B_{10}C_3O_2SFe$ and the band-gap energy was approximated by 5.6 eV based on the UV absorption spectra of M9-COOH. The band-gap energy of the carborane cluster in M9 lies several eV higher and thus was not taken into account and the thiol group was approximated by that of organic thiols with the band-gap energy being close to 5.6 eV again.[122]–[125]

Geometric model of densely packed molecules confined on a surface

Computed structure of M1-COOH has been used, for the X-ray structures of either M1-COOH or M9-COOH were not available at the time. The X-ray structures were obtained later and proved well in the error of the model used. The M1-COOH structure was used as a set of atomic coordinates in a .xyz file from which the data have been imported to EXCEL software, the .xyz files of M1-COOH and M9-COOH structures obtained by quantum computation as well as from X-ray crystallography are presented in the supporting information. Translation and rotation transformation matrices were then used to move the molecule such that the S atom is in the beginning of the coordination system, the molecular axis intersecting the S atom and the antipodal B atom is in the z coordinate axis and the plane intersecting the S atom, the antipodal B atom and the C atom, to which the −COOH group is bonded, are in the yz plane.

Rotation transformation matrix together with Van der Waals atomic radii were used to find the most dense packing of molecules on the surface. For isotropic packing the molecule was rotated around the x axis to scan for the tilt in which the distance of the most distant component (atom coordinates + VdW atomic radii) from the z axis acquires the smallest value, this distance is the nearest neighbor distance. The method was easily reversed to find the tilt for isotropic packing with the nearest neighbor distance of 8.6 Å. To find the most dense anisotropic packing the molecule was rotated in the same fashion but the value scanned was the sum of the distances of the two most distant components (atom coordinates + VdW atomic radii) from the z axis in the yz plane in the positive and negative directions on the y axis, yielding the nearest neighbor distance in the direction of the tilt, the molecule was then rotated around the z axis by 60º and again the sum of the distances of the two most distant components from the z axis in the yz plane in the positive and negative directions on the y axis yielded the nearest neighbor distance for the next direction with translation periodicity. The molecule was then rotated by 60º again and the process was repeated to yield the nearest neighbor distance for the last relevant direction.

The method doesn't take in to account the vertical profile of the molecule. This might lead to more dense packing in the direction of the tilt for the model with anisotropic packing, but the problem was not addressed since the model proved to yield too dense packing anyway. This doesn't affect the results for the model with isotropic packing.

Calculation of the molecular structure of M1-COOH

Quantum chemistry calculations were performed by the NWChem package.[126] The geometries were optimized by the means of the density functional theory with the hybrid exchange–correlation functional PBE0.[127]–[130] Jensen's triple–zeta polarization consistent basis set pc-2 was used.[131]

Calculation of the dipole-dipole interaction enthalpy

Dipole-dipole interaction enthalpy was calculated as interaction energy of molecular dipole, $\vec{p_m}$ in electric field $\vec{E}$:

$$\Delta H_{\text{int}} = \Delta U_{\text{int}} = -\vec{p_m} \cdot \vec{E} \cdot N_A \tag{15}$$

where N_A is the Avogadro's number and $\vec{E}$ is the sum of contributions from neighboring molecular dipoles to the local electric field:

$$\vec{E} = \frac{1}{4 \cdot \pi \cdot \varepsilon_0} \sum_n \left[\frac{\vec{p_n}}{r_n^3} \right] \tag{16}$$

where ε_0 is the permittivity of vacuum, $\vec{p_n}$ is the molecular dipole of neighboring molecule n and r_n is the distance of the molecule n from the molecule m. The second term normally occurring in the dipole induced electric field equation is disregarded as the molecular dipole is perpendicular to the surface, making the term equal to 0.

The summation of the local electric field of pristine O1,2 and O9,12 SAMs was calculated for up to 7 concentric hexagonal rings and then approximated by a power function. The summation of the local electric field of mixed SAMs was calculated up to 6 concentric hexagonal rings and then truncated as the higher terms were becoming negligible. Two sites with different contribution and weight were calculated and averaged for the mixed SAM with 2:1 ratio. Periodic patterns with unit cells as depicted in **Fig. 15 A** and **B**, were used for the 1:1 and 2:1 ratios respectively.
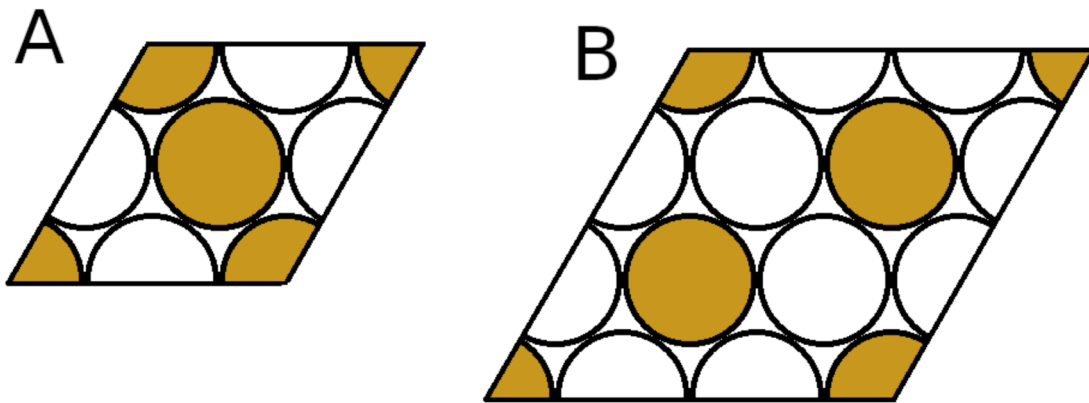
Figure 2: Unit cells used in the periodic surface patterns from which dipole-dipole interaction enthalpy was calculated. A) pattern used for the 1:1 ratio; B) pattern used for the 2:1 ratio.

The effect of Au-S bonding on the magnitude of the molecular dipoles as well as the effect of electrostatic induction in the substrate and in the molecules has been neglected.

Literature

[1] W. Bigelow, D. Pickett, and W. Zisman, 'Oleophobic Monolayers .1. Films Adsorbed from Solution in Non-Polar Liquids', *J. Colloid Sci.*, vol. 1, no. 6, pp. 513–538, 1946.

[2] A. Ulman, 'Formation and Structure of Self-Assembled Monolayers', *Chem. Rev.*, vol. 96, no. 4, pp. 1533–1554, Jan. 1996.

[3] R. K. Smith, P. A. Lewis, and P. S. Weiss, 'Patterning self-assembled monolayers', *Prog. Surf. Sci.*, vol. 75, no. 1–2, pp. 1–68, Jun. 2004.

[4] N. K. Chaki and K. Vijayamohanan, 'Self-assembled monolayers as a tunable platform for biosensor applications', *Biosens. Bioelectron.*, vol. 17, no. 1, pp. 1–12, Jan. 2002.

[5] J. M. Buriak, 'Organometallic Chemistry on Silicon and Germanium Surfaces', *Chem. Rev.*, vol. 102, no. 5, pp. 1271–1308, May 2002.

[6] G. Hahner, R. Hofer, and I. Klingenfuss, 'Order and orientation in self-assembled long chain alkanephosphate monolayers adsorbed on metal oxide surfaces', *Langmuir*, vol. 17, no. 22, pp. 7047–7052, Oct. 2001.

[7] L. Srisombat, A. C. Jamison, and T. R. Lee, 'Stability: A key issue for self-assembled monolayers on gold as thin-film coatings and nanoparticle protectants', *Colloids Surf. -Physicochem. Eng. Asp.*, vol. 390, no. 1–3, pp. 1–19, Oct. 2011.

[8] X. Cheng, S. B. Lowe, P. J. Reece, and J. J. Gooding, 'Colloidal silicon quantum dots: from preparation to the modification of self-assembled monolayers (SAMs) for bio-applications', *Chem. Soc. Rev.*, vol. 43, no. 8, pp. 2680–2700, 2014.

[9] Y. Song, R. P. Nair, M. Zou, and Y. Wang, 'Superhydrophobic Surfaces Produced by Applying a Self-Assembled Monolayer to Silicon Micro/Nano-Textured Surfaces', *Nano Res.*, vol. 2, no. 2, pp. 143–150, Feb. 2009.

[10] S. G. Moussa *et al.*, 'Experimental and Theoretical Characterization of Adsorbed Water on Self-Assembled Monolayers: Understanding the Interaction of Water with Atmospherically Relevant Surfaces', *J. Phys. Chem. A*, vol. 113, no. 10, pp. 2060–2069, Mar. 2009.

[11] M. K. Chaudhury, 'Adhesion and friction of self-assembled organic monolayers', *Curr. Opin. Colloid Interface Sci.*, vol. 2, no. 1, pp. 65–69, Feb. 1997.

[12] J. E. Houston and H. I. Kim, 'Adhesion, friction, and mechanical properties of functionalized alkanethiol self-assembled monolayers', *Acc. Chem. Res.*, vol. 35, no. 7, pp. 547–553, Jul. 2002.

[13] S. Watson, M. Nie, L. Wang, and K. Stokes, 'Challenges and developments of self-assembled monolayers and polymer brushes as a green lubrication solution for tribological applications', *Rsc Adv.*, vol. 5, no. 109, pp. 89698–89730, 2015.

[14] R. K. Smith, P. A. Lewis, and P. S. Weiss, 'Patterning self-assembled monolayers', *Prog. Surf. Sci.*, vol. 75, no. 1–2, pp. 1–68, erven 2004.

[15] J. N. Hohman, S. A. Claridge, M. Kim, and P. S. Weiss, 'Cage molecules for self-assembly', *Mater. Sci. Eng. R Rep.*, vol. 70, no. 3–6, pp. 188–208, Nov. 2010.

[16] T. Konishi and K. Yamaguchi, 'Surface Control of a Photoresponsive Self-Assembled Monolayer and Selective Deposition of Ag Nanoparticulate Ink', *Bull. Chem. Soc. Jpn.*, vol. 89, no. 4, pp. 424–429, Apr. 2016.

[17] P. Dutta, P. J. Chapman, P. G. Datskos, and M. J. Sepaniak, 'Characterization of ligand-functionalized microcantilevers for metal ion sensing', *Anal. Chem.*, vol. 77, no. 20, pp. 6601–6608, Oct. 2005.

[18] H. F. Ji, T. Thundat, R. Dabestani, G. M. Brown, P. F. Britt, and P. V. Bonnesen, 'Ultrasensitive detection of CrO42- using a microcantilever sensor', *Anal. Chem.*, vol. 73, no. 7, pp. 1572–1576, Apr. 2001.

[19] A. Hasan and L. M. Pandey, 'Review: Polymers, Surface-Modified Polymers, and Self Assembled Monolayers as Surface-Modifying Agents for Biomaterials', *Polym.-Plast. Technol. Eng.*, vol. 54, no. 13, pp. 1358–1378, Sep. 2015.

[20] C. C. Barrias, M. C. L. Martins, G. Almeida-Porada, M. A. Barbosa, and P. L. Granja, 'The correlation between the adsorption of adhesive proteins and cell behaviour on hydroxyl-methyl mixed self-assembled monolayers', *Biomaterials*, vol. 30, no. 3, pp. 307–316, Jan. 2009.

[21] J. E. Raynor, J. R. Capadona, D. M. Collard, T. A. Petrie, and A. J. Garcia, 'Polymer brushes and self-assembled monolayers: Versatile platforms to control cell adhesion to biomaterials (Review)', *Biointerphases*, vol. 4, no. 2, pp. FA3–FA16, Jun. 2009.

[22] G. Mani *et al.*, 'Drug delivery from gold and titanium surfaces using self-assembled monolayers', *Biomaterials*, vol. 29, no. 34, pp. 4561–4573, Dec. 2008.

[23] A. Shakiba, O. Zenasni, M. D. Marquez, and T. R. Lee, 'Advanced drug delivery via self-assembled monolayer-coated nanoparticles', *Aims Bioeng.*, vol. 4, no. 2, pp. 275–299, 2017.

[24] F. Boeke, K. Schickle, and H. Fischer, 'Biological Activation of Inert Ceramics: Recent Advances Using Tailored Self-Assembled Monolayers on Implant Ceramic Surfaces', *Materials*, vol. 7, no. 6, pp. 4473–4492, Jun. 2014.

[25] N. Yoshino and T. Teranaka, 'Synthesis of silane coupling agents containing fluorocarbon chain and applications to dentistry: Plaque-controlling surface modifiers', *J. Biomater. Sci.-Polym. Ed.*, vol. 8, no. 8, pp. 623–653, 1997.

[26] S. C. D'Andrea, K. S. Iyer, I. Luzinov, and A. Y. Fadeev, 'Self-assembled monolayers of organophosphonic acids supported on teeth', *Colloids Surf. B-Biointerfaces*, vol. 32, no. 3, pp. 235–243, Nov. 2003.

[27] L. Tack, K. Schickle, F. Boeke, and H. Fischer, 'Immobilization of specific proteins to titanium surface using self-assembled monolayer technique', *Dent. Mater.*, vol. 31, no. 10, pp. 1169–1179, Oct. 2015.

[28] H. Li, W. Huang, Y. Zhang, and M. Zhong, 'Biomimetic synthesis of enamel-like hydroxyapatite on self-assembled monolayers', *Mater. Sci. Eng. C-Biomim. Supramol. Syst.*, vol. 27, no. 4, pp. 756–761, May 2007.

[29] W. Knoll, I. Koeper, R. Naumann, and E.-K. Sinner, 'Tethered bimolecular lipid membranes - A novel model membrane platform', *Electrochimica Acta*, vol. 53, no. 23, pp. 6680–6689, Oct. 2008.

[30] A. L. Eckermann, D. J. Feld, J. A. Shaw, and T. J. Meade, 'Electrochemistry of redox-active self-assembled monolayers', *Coord. Chem. Rev.*, vol. 254, no. 15–16, pp. 1769–1802, Aug. 2010.

[31] D. Samanta and A. Sarkar, 'Immobilization of bio-macromolecules on self-assembled monolayers: methods and sensor applications', *Chem. Soc. Rev.*, vol. 40, no. 5, pp. 2567–2592, 2011.

[32] R. S. Freire, C. A. Pessoa, L. D. Mello, and L. T. Kubota, 'Direct electron transfer: an approach for electrochemical biosensors with higher selectivity and sensitivity', *J. Braz. Chem. Soc.*, vol. 14, no. 2, pp. 230–243, Apr. 2003.

[33] D. Chen and J. Li, 'Interfacial design and functionization on metal electrodes through self-assembled monolayers', *Surf. Sci. Rep.*, vol. 61, no. 11, pp. 445–463, Dec. 2006.

[34] T. Kondo and K. Uosaki, 'Self-assembled monolayers (SAMs) with photo-functionalities', *J. Photochem. Photobiol. C-Photochem. Rev.*, vol. 8, no. 1, pp. 1–17, Mar. 2007.

[35] B. A. Mantooth and P. S. Weiss, 'Fabrication, assembly, and characterization of molecular electronic components', *Proc. IEEE*, vol. 91, no. 11, pp. 1785–1802, Nov. 2003.

[36] S. Casalini, C. A. Bortolotti, F. Leonardi, and F. Biscarini, 'Self-assembled monolayers in organic electronics', *Chem. Soc. Rev.*, vol. 46, no. 1, pp. 40–71, Jan. 2017.

[37] D. Liu and Q. Miao, 'Recent progress in interface engineering of organic thin film transistors with self-assembled monolayers', *Mater. Chem. Front.*, vol. 2, no. 1, pp. 11–21, Jan. 2018.

[38] C. A. Schoenbaum, D. K. Schwartz, and J. W. Medlin, 'Controlling the Surface Environment of Heterogeneous Catalysts Using Self-Assembled Monolayers', *Acc. Chem. Res.*, vol. 47, no. 4, pp. 1438–1445, Apr. 2014.

[39] A. Turchanin and A. Goelzhaeuser, 'Carbon nanomembranes from self-assembled monolayers: Functional surfaces without bulk', *Prog. Surf. Sci.*, vol. 87, no. 5–8, pp. 108–162, Aug. 2012.

[40] A. Turchanin, 'Graphene Growth by Conversion of Aromatic Self-Assembled Monolayers', *Ann. Phys.*, vol. 529, no. 11, p. 1700168, Nov. 2017.

[41] A. R. Bishop and R. G. Nuzzo, 'Self-assembled monolayers: Recent developments and applications', *Curr. Opin. Colloid Interface Sci.*, vol. 1, no. 1, pp. 127–136, Feb. 1996.

[42] S. W. Tam-Chang and I. Iverson, 'Applications of self-assembled monolayers (SAMs) of alkanethiolates on gold', *Adsorpt. Its Appl. Ind. Environ. Prot. Vol Appl. Ind.*, vol. 120, pp. 917–950, 1999.

[43] J. J. Gooding, F. Mearns, W. R. Yang, and J. Q. Liu, 'Self-assembled monolayers into the 21(st) century: Recent advances and applications', *Electroanalysis*, vol. 15, no. 2, pp. 81–96, Feb. 2003.

[44] J. C. Love, L. A. Estroff, J. K. Kriebel, R. G. Nuzzo, and G. M. Whitesides, 'Self-assembled monolayers of thiolates on metals as a form of nanotechnology', *Chem. Rev.*, vol. 105, no. 4, pp. 1103–1169, Apr. 2005.

[45] K. Ariga, J. P. Hill, M. V. Lee, A. Vinu, R. Charvet, and S. Acharya, 'Challenges and breakthroughs in recent research on self-assembly', *Sci. Technol. Adv. Mater.*, vol. 9, no. 1, p. 014109, Mar. 2008.

[46] E. Wood, 'Vocabulary of Surface Crystallography', *J. Appl. Phys.*, vol. 35, no. 4, pp. 1306-, 1964.

[47] R. Nuzzo and D. Allara, 'Adsorption of Bifunctional Organic Disulfides on Gold Surfaces', *J. Am. Chem. Soc.*, vol. 105, no. 13, pp. 4481–4483, 1983.

[48] N. Sandhyarani and T. Pradeep, 'Current understanding of the structure, phase transitions and dynamics of self-assembled monolayers on two- and three-dimensional surfaces', *Int. Rev. Phys. Chem.*, vol. 22, no. 2, pp. 221–262, Jun. 2003.

[49] C. Vericat, M. E. Vela, and R. C. Salvarezza, 'Self-assembled monolayers of alkanethiols on Au(111): surface structures, defects and dynamics', *Phys. Chem. Chem. Phys.*, vol. 7, no. 18, pp. 3258–3268, 2005.

[50] C. Vericat, M. E. Vela, G. Benitez, P. Carro, and R. C. Salvarezza, 'Self-assembled monolayers of thiols and dithiols on gold: new challenges for a well-known system', *Chem. Soc. Rev.*, vol. 39, no. 5, pp. 1805–1834, 2010.

[51] C. Vericat *et al.*, 'Self-assembled monolayers of thiolates on metals: a review article on sulfur-metal chemistry and surface structures', *Rsc Adv.*, vol. 4, no. 53, pp. 27730–27754, 2014.

[52] H. Biebuyck, C. Bian, and G. Whitesides, 'Comparison of Organic Monolayers on Polycrystalline Gold Spontaneously Assembled from Solutions Containing Dialkyl Disulfides or Alkenethiols', *Langmuir*, vol. 10, no. 6, pp. 1825–1831, Jun. 1994.

[53] R. Nuzzo, B. Zegarski, and L. Dubois, 'Fundamental-Studies of the Chemisorption of Organosulfur Compounds on Au(111) - Implications for Molecular Self-Assembly on Gold Surfaces', *J. Am. Chem. Soc.*, vol. 109, no. 3, pp. 733–740, Feb. 1987.

[54] W. Azzam, 'Temperature-induced phase transition; Polymorphism in BP2 SAMs on Au(111)', *Cent. Eur. J. Chem.*, vol. 7, no. 4, pp. 884–899, Dec. 2009.

[55] F. von Wrochem, F. Scholz, A. Yasuda, and J. M. Wessels, 'Probing Structure and Molecular Conductance in Highly Ordered Benzyl Mercaptan Monolayers', *J. Phys. Chem. C*, vol. 113, no. 28, pp. 12395–12401, Jul. 2009.

[56] J. B. Schlenoff, M. Li, and H. Ly, 'Stability and self-exchange in alkanethiol monolayers', *J. Am. Chem. Soc.*, vol. 117, no. 50, pp. 12528–12536, Dec. 1995.

[57] C. Woll, S. Chiang, R. Wilson, and P. Lippel, 'Determination of Atom Positions at Stacking-Fault Dislocations on Au(111) by Scanning Tunneling Microscopy', *Phys. Rev. B*, vol. 39, no. 11, pp. 7988–7991, Apr. 1989.

[58] P. Maksymovych, O. Voznyy, D. B. Dougherty, D. C. Sorescu, and J. T. Yates, 'Gold adatom as a key structural component in self-assembled monolayers of organosulfur molecules on Au(111)', *Prog. Surf. Sci.*, vol. 85, no. 5–8, pp. 206–240, Aug. 2010.

[59] N. Arisnabarreta, G. D. Ruano, M. Lingenfelder, E. M. Patrito, and F. P. Cometto, 'Comparative Study of the Adsorption of Thiols and Selenols on Au(111) and Au(100)', *Langmuir*, vol. 33, no. 48, pp. 13733–13739, Dec. 2017.

[60] L. Dubois and R. Nuzzo, 'Synthesis, Structure, and Properties of Model Organic-Surfaces', *Annu. Rev. Phys. Chem.*, vol. 43, pp. 437–463, 1992.

[61] R. Valiokas, M. Ostblom, S. Svedhem, S. C. T. Svensson, and B. Liedberg, 'Temperature-driven phase transitions in oligo(ethylene glycol)-terminated self-assembled monolayers', *J. Phys. Chem. B*, vol. 104, no. 32, pp. 7565–7569, Aug. 2000.

[62] P. Fenter, P. Eisenberger, and K. Liang, 'Chain-Length Dependence of the Structures and Phases of Ch3(ch2)n-1sh Self-Assembled on Au(111)', *Phys. Rev. Lett.*, vol. 70, no. 16, pp. 2447–2450, Apr. 1993.

[63] E. Jose Juarez-Perez, M. Granier, C. Vinas, P. H. Mutin, and R. Nunez, 'Grafting of Metallacarboranes onto Self-Assembled Monolayers Deposited on Silicon Wafers', *Chem.- Asian J.*, vol. 7, no. 2, pp. 277–281, Feb. 2012.

[64] V. Štengl, S. Bakardjieva, M. Bakardjiev, B. Štíbr, and M. Kormunda, 'Carborane functionalized graphene oxide, a precursor for conductive self-assembled monolayers', *Carbon*, vol. 67, pp. 336–343, Feb. 2014.

[65] A. C. Serino *et al.*, 'Work Function Control of Germanium through Carborane-Carboxylic Acid Surface Passivation', *Acs Appl. Mater. Interfaces*, vol. 9, no. 40, pp. 34592–34596, Oct. 2017.

[66] M. Ito *et al.*, 'A novel method for creation of free volume in a one-component self-assembled monolayer. Dramatic size effect of para-carborane', *J. Mater. Chem.*, vol. 15, no. 4, pp. 478–483, Jan. 2005.

[67] E. Ito, H. Ito, H. Kang, T. Hayashi, M. Hara, and J. Noh, 'Influence of Surface Morphology and Substrate on Thermal Stability and Desorption Behavior of

Octanethiol Self-Assembled Monolayers: Cu, Ag, and Au', *J. Phys. Chem. C*, vol. 116, no. 33, pp. 17586–17593, Aug. 2012.

[68] T. Base *et al.*, 'Carboranethiol-modified gold surfaces. A study and comparison of modified cluster and flat surfaces', *Langmuir*, vol. 21, no. 17, pp. 7776–7785, Aug. 2005.

[69] T. Base *et al.*, 'Gold micrometer crystals modified with carboranethiol derivatives', *J. Phys. Chem. C*, vol. 112, no. 37, pp. 14446–14455, Sep. 2008.

[70] J. N. Hohman *et al.*, 'Self-Assembly of Carboranethiol Isomers on Au{111}: Intermolecular Interactions Determined by Molecular Dipole Orientations', *ACS Nano*, vol. 3, no. 3, pp. 527–536, Mar. 2009.

[71] F. von Wrochem *et al.*, 'High-Band-Gap Polycrystalline Monolayers of a 12-Vertex p-Carborane on Au(111)', *J. Phys. Chem. Lett.*, vol. 1, no. 24, pp. 3471–3477, Dec. 2010.

[72] F. Scholz *et al.*, 'Permethylated 12-Vertex p-Carborane Self-Assembled Monolayers', *J. Phys. Chem. C*, vol. 115, no. 46, pp. 22998–23007, Nov. 2011.

[73] J. F. Luebben, T. Base, P. Rupper, T. Kuenniger, J. Machacek, and S. Guimond, 'Tuning the surface potential of Ag surfaces by chemisorption of oppositely-oriented thiolated carborane dipoles', *J. Colloid Interface Sci.*, vol. 354, no. 1, pp. 168–174, Feb. 2011.

[74] A. Vetushka *et al.*, 'Adsorption of oriented carborane dipoles on a silver surface', *Phys. Status Solidi B-Basic Solid State Phys.*, vol. 253, no. 3, pp. 591–600, Mar. 2016.

[75] J. J. Schwartz *et al.*, 'Surface Dipole Control of Liquid Crystal Alignment', *J. Am. Chem. Soc.*, vol. 138, no. 18, pp. 5957–5967, May 2016.

[76] J. C. Thomas *et al.*, 'Self-Assembled p-Carborane Analogue of p-Mercaptobenzoic Acid on Au{111}', *Chem. Mater.*, vol. 27, no. 15, pp. 5425–5435, Aug. 2015.

[77] J. C. Thomas *et al.*, 'Acid–Base Control of Valency within Carboranedithiol Self-Assembled Monolayers: Molecules Do the Can-Can', *ACS Nano*, vol. 12, no. 3, pp. 2211–2221, Mar. 2018.

[78] A. M. Cioran *et al.*, 'Mercaptocarborane-Capped Gold Nanoparticles: Electron Pools and Ion Traps with Switchable Hydrophilicity', *J. Am. Chem. Soc.*, vol. 134, no. 1, pp. 212–221, Jan. 2012.

[79] A. M. Cioran, F. Teixidor, Ž. Krpetić, M. Brust, and C. Viñas, 'Preparation and characterization of Au nanoparticles capped with mercaptocarboranyl clusters', *Dalton Trans.*, vol. 43, no. 13, pp. 5054–5061, Mar. 2014.

[80] T. Base *et al.*, 'Carborane-thiol-silver interactions. A comparative study of the molecular protection of silver surfaces', *Surf. Coat. Technol.*, vol. 204, no. 16–17, pp. 2639–2646, May 2010.

[81] T. Base, Z. Bastl, V. Havranek, J. Machacek, J. Langecker, and V. Malina, 'Carboranedithiols: Building Blocks for Self-Assembled Monolayers on Copper Surfaces', *Langmuir*, vol. 28, no. 34, pp. 12518–12526, Aug. 2012.

[82] A. Yavuz, N. Sohrabnia, A. Yilmaz, and M. F. Danışman, 'Mixed carboranethiol self-assembled monolayers on gold surfaces', *Appl. Surf. Sci.*, vol. 413, pp. 233–241, Aug. 2017.

[83] E. Mete, A. Yılmaz, and M. F. Danışman, 'A van der Waals density functional investigation of carboranethiol self-assembled monolayers on Au(111)', *Phys. Chem. Chem. Phys.*, vol. 18, no. 18, pp. 12920–12927, May 2016.

[84] Y. T. Tao, C. C. Wu, J. Y. Eu, W. L. Lin, K. C. Wu, and C. H. Chen, 'Structure evolution of aromatic-derivatized thiol monolayers on evaporated gold', *Langmuir*, vol. 13, no. 15, pp. 4018–4023, Jul. 1997.

[85] T. Sawaguchi, F. Mizutani, S. Yoshimoto, and I. Taniguchi, 'Voltammetric and in situ STM studies on self-assembled monolayers of 4-mercaptopyridine, 2-mercaptopyridine and thiophenol on Au(111) electrodes', *Electrochimica Acta*, vol. 45, no. 18, pp. 2861–2867, 2000.

[86] A. A. Dameron, J. W. Ciszek, J. M. Tour, and P. S. Weiss, 'Effects of hindered internal rotation on packing and conductance of self-assembled monolayers', *J. Phys. Chem. B*, vol. 108, no. 43, pp. 16761–16767, Oct. 2004.

[87] D. Kafer, G. Witte, P. Cyganik, A. Terfort, and C. Woll, 'A comprehensive study of self-assembled monolayers of anthracenethiol on gold: Solvent effects, structure, and stability', *J. Am. Chem. Soc.*, vol. 128, no. 5, pp. 1723–1732, Feb. 2006.

[88] S. Reese and M. A. Fox, 'Self-assembled monolayers on gold of thiols incorporating conjugated terminal groups', *J. Phys. Chem. B*, vol. 102, no. 49, pp. 9820–9824, Dec. 1998.

[89] S. D. Evans, E. Urankar, A. Ulman, and N. Ferris, 'Self-assembled monolayers of alkanethiols containing a polar aromatic group: effects of the dipole position on molecular packing, orientation, and surface wetting properties', *J. Am. Chem. Soc.*, vol. 113, no. 11, pp. 4121–4131, May 1991.

[90] J. F. Kang, S. Liao, R. Jordan, and A. Ulman, 'Mixed Self-assembled Monolayers of Rigid Biphenyl Thiols: Impact of Solvent and Dipole Moment', *J. Am. Chem. Soc.*, vol. 120, no. 37, pp. 9662–9667, Sep. 1998.

[91] J. F. Kang, A. Ulman, S. Liao, and R. Jordan, 'Mixed self-assembled monolayers of highly polar rigid biphenyl thiols', *Langmuir*, vol. 15, no. 6, pp. 2095–2098, Mar. 1999.

[92] J. N. Hohman *et al.*, 'Self-Assembly of Carboranethiol Isomers on Au{111}: Intermolecular Interactions Determined by Molecular Dipole Orientations', *ACS Nano*, vol. 3, no. 3, pp. 527–536, Mar. 2009.

[93] J. C. Thomas *et al.*, 'Defect-Tolerant Aligned Dipoles within Two-Dimensional Plastic Lattices', *Acs Nano*, vol. 9, no. 5, pp. 4734–4742, May 2015.

[94] T. Sawaguchi, Y. Sato, and F. Mizutani, 'Ordered structures of self-assembled monolayers of 3-mercaptopropionic acid on Au(111): in situ scanning tunneling microscopy study', *Phys. Chem. Chem. Phys.*, vol. 3, no. 16, pp. 3399–3404, 2001.

[95] T. J. Mullen, A. A. Dameron, A. M. Andrews, and P. S. Weiss, 'Selecting and driving monolayer structures through tailored intermolecular interactions', *Aldrichimica Acta*, vol. 40, no. 1, pp. 21–31, 2007.

[96] P. Dutta, P. J. Chapman, P. G. Datskos, and M. J. Sepaniak, 'Characterization of ligand-functionalized microcantilevers for metal ion sensing', *Anal. Chem.*, vol. 77, no. 20, pp. 6601–6608, Oct. 2005.

[97] S.-H. Hsu, D. N. Reinhoudt, J. Huskens, and A. H. Velders, 'Lateral interactions at functional monolayers', *J. Mater. Chem.*, vol. 21, no. 8, pp. 2428–2444, 2011.

[98] J. Poppenberg *et al.*, 'Successive coordination of palladium(II)-ions and terpyridine-ligands to a pyridyl-terminated self-assembled monolayer on gold', *Surf. Sci.*, vol. 606, no. 3–4, pp. 367–377, Feb. 2012.

[99] C. H.-H. Traulsen *et al.*, 'Intermixed Terpyridine-Functionalized Monolayers on Gold: Nonlinear Relationship between Terpyridyl Density and Metal Ion Coordination Properties', *Langmuir*, vol. 28, no. 29, pp. 10755–10763, Jul. 2012.

[100] J. Scofield, 'Hartree-Slater Subshell Photoionization Cross-Sections at 1254 and 1487ev', *J. Electron Spectrosc. Relat. Phenom.*, vol. 8, no. 2, pp. 129–137, 1976.

[101] J. Yeh and I. Lindau, 'Atomic Subshell Photoionization Cross-Sections and Asymmetry Parameters - 1 Less-Than-or-Equal-to Z Less-Than-or-Equal-to 103', *At. Data Nucl. Data Tables*, vol. 32, no. 1, pp. 1–155, 1985.

[102]   M. B. Trzhaskovskaya, Y. I. Kharitonov, V. I. Nefedov, and V. G. Yarzhemskii, 'Study of parameters of the angular distribution of photoelectrons in the relativistic quadrupole approximation', *Opt. Spectrosc.*, vol. 88, no. 4, pp. 489–497, Apr. 2000.

[103]   V. I. Nefedov, V. G. Yarzhemsky, and M. B. Trzhaskovskaya, 'The influence of relaxation and nondipole effects on the intensity of X-ray photoelectron spectra', *Bull. Russ. Acad. Sci. Phys.*, vol. 72, no. 4, pp. 423–428, Apr. 2008.

[104]   'NPL System for the intensity calibration of X-ray Photoelectron Spectrometers, X1 (NPL, Teddington, Middlesex TW11 0LW, UK), see http://www.npl.co.uk/nanoanalysis and follow links.'

[105]   M. Seah and G. Smith, 'Quantitative Aes and Xps - Determination of the Electron Spectrometer Transmission Function and the Detector Sensitivity Energy Dependencies for the Production of True Electron-Emission Spectra in Aes and Xps', *Surf. Interface Anal.*, vol. 15, no. 12, pp. 751–766, Dec. 1990.

[106]   C. J. Powell and A. Jablonski, 'Progress in quantitative surface analysis by X-ray photoelectron spectroscopy: Current status and perspectives', *J. Electron Spectrosc. Relat. Phenom.*, vol. 178–179, pp. 331–346, May 2010.

[107]   M. P. Seah and I. S. Gilmore, 'Quantitative AES. VIII: Analysis of Auger electron intensities from elemental data in a digital Auger database', *Surf. Interface Anal.*, vol. 26, no. 12, pp. 908–929, Nov. 1998.

[108]   M. P. Seah, I. S. Gilmore, and S. J. Spencer, 'Quantitative XPS I. Analysis of X-ray photoelectron intensities from elemental data in a digital photoelectron database', *J. Electron Spectrosc. Relat. Phenom.*, vol. 120, no. 1–3, pp. 93–111, Oct. 2001.

[109]   M. P. Seah and I. S. Gilmore, 'Quantitative x-ray photoelectron spectroscopy: Quadrupole effects, shake-up, Shirley background, and relative sensitivity factors from a database of true x-ray photoelectron spectra', *Phys. Rev. B*, vol. 73, no. 17, p. 174113, May 2006.

[110]   C. Wagner, L. Davis, M. Zeller, J. Taylor, R. Raymond, and L. Gale, 'Empirical Atomic Sensitivity Factors for Quantitative-Analysis by Electron-Spectroscopy for Chemical-Analysis', *Surf. Interface Anal.*, vol. 3, no. 5, pp. 211–225, 1981.

[111]S. Tougaard, 'Energy loss in XPS: Fundamental processes and applications for quantification, non-destructive depth profiling and 3D imaging', *J. Electron Spectrosc. Relat. Phenom.*, vol. 178, pp. 128–153, May 2010.

[112]   S. Tougaard and C. Jansson, 'Background Correction in Xps - Comparison of Validity of Different Methods', *Surf. Interface Anal.*, vol. 19, no. 1–12, pp. 171–174, Jun. 1992.

[113]   C. van der Marel, M. Yidirim, and H. R. Stapert, 'Multilayer approach to the quantitative analysis of x-ray photoelectron spectroscopy results: Applications to ultrathin SiO2 on Si and to self-assembled monolayers on gold', *J. Vac. Sci. Technol. A*, vol. 23, no. 5, pp. 1456–1470, Oct. 2005.

[114]   A. Jablonski and C. J. Powell, 'The electron attenuation length revisited', *Surf. Sci. Rep.*, vol. 47, no. 2–3, pp. 35–91, 2002.

[115]   Paul S. Weiss, Tomas Base, Wang, Dominic P Goronzy, John C. Thomas, and Jan Stanek, 'Not yet published data from international collaboration of our laboratory.'

[116]   J. Staněk, T. Baše, P. Matějíček, J. Vohlídal, and K. Univerzita, 'MANIFESTATION OF POLAR EFFECTS IN BIFUNCTIONAL CARBORANYL MOIETIES', 2015.

[117]   C. J. Carrell, H. L. Carrell, J. Erlebacher, and J. P. Glusker, 'Structural aspects of metal ion carboxylate interactions', *J. Am. Chem. Soc.*, vol. 110, no. 26, pp. 8651–8656, Dec. 1988.

[118]   R. D. Shannon, 'Revised effective ionic radii and systematic studies of interatomic distances in halides and chalcogenides', *Acta Crystallogr. Sect. A*, vol. 32, no. 5, pp. 751–767.

[119]   C. Traunsteiner, S. Sek, V. Huber, C. Valero-Vidal, and J. Kunze-Liebhäuser, 'Laccase immobilized on a mixed thiol monolayer on Au(111) – structure-dependent activity towards oxygen reduction', *Electrochimica Acta*, vol. 213, pp. 761–770, Sep. 2016.

[120]   C. J. Powell and A. Jablonski, *NIST Electron Effective-Attenuation-Length Database*, Version 1.3. Gaithersburg: National Institute of Standards and Technology, 2011.

[121]   C. J. Powell and A. Jablonski, *NIST Electron Inelastic-Mean-Free-Path Database*, Version 1.2. Gaithersburg: National Institute of Standards and Technology, 2010.

[122]   E. A. Dikusar *et al.*, 'Functionalyzed Nitrogen-and Phosphorus-containing Salts of Cycloalkanecarboxylic and Carboranecarboxylic Acids', *Russ. J. Gen. Chem.*, vol. 75, no. 1, pp. 58–68, Jan. 2005.

[123]   T. Vondrák, J. Plešek, S. Heřmánek, and B. Štíbr, 'Charge distribution in icosahedral carboranes: A UV photoelectron spectroscopic study', *Polyhedron*, vol. 8, no. 6, pp. 805–811, Jan. 1989.

[124]   A. V. Okotrub, L. G. Bulusheva, and V. V. Volkov, 'Electron interactions in the closo-carboranes 1,2- and 1,7-C2B10H12', *J. Mol. Struct.*, vol. 520, no. 1, pp. 33–38, Mar. 2000.

[125]   D. F. Sheraton and F. E. Murray, 'Quantum yields in the photolytic oxidation of some sulphur compounds', *Can. J. Chem.*, vol. 59, no. 18, pp. 2750–2754, Sep. 1981.

[126]   M. Valiev *et al.*, 'NWChem: A comprehensive and scalable open-source solution for large scale molecular simulations', *Comput. Phys. Commun.*, vol. 181, no. 9, pp. 1477–1489, Sep. 2010.

[127]   C. Adamo and V. Barone, 'Toward reliable density functional methods without adjustable parameters: The PBE0 model', *J. Chem. Phys.*, vol. 110, no. 13, pp. 6158–6170, Mar. 1999.

[128]   C. Adamo and V. Barone, 'Inexpensive and accurate predictions of optical excitations in transition-metal complexes: the TDDFT/PBE0 route', *Theor. Chem. Acc.*, vol. 105, no. 2, pp. 169–172, Dec. 2000.

[129]   C. Adamo and V. Barone, 'Physically motivated density functionals with improved performances: The modified Perdew–Burke–Ernzerhof model', *J. Chem. Phys.*, vol. 116, no. 14, pp. 5933–5940, Mar. 2002.

[130]   'Accurate excitation energies from time-dependent density functional theory: Assessing the PBE0 model: The Journal of Chemical Physics: Vol 111, No 7'. [Online]. Available: https://aip.scitation.org/doi/10.1063/1.479571. [Accessed: 27-Jun-2018].

[131]   F. Jensen, 'Unifying General and Segmented Contracted Basis Sets. Segmented Polarization Consistent Basis Sets', *J. Chem. Theory Comput.*, vol. 10, no. 3, pp. 1074–1085, Mar. 2014.

[132]   'Copyright © 2005 Casa Software Ltd'. [Online]. Available: http://www.casaxps.com/.